REPORT DOCUMENTATION PAGE

Form Approved OMB No. 0704-0188

Public reporting burden for this collection of information is estimated to average 1 hour per response, including the time for reviewing instructions, searching existing data sources, gathering and maintaining the data needed, and completing and reviewing the collection of information. Send comments regarding this burden estimate or any other aspect of this collection of information, including suggestions for reducing the burden, to Department of Defense, Washington Headquarters Services, Directorate for Information Operations and Reports (0704-0188), 1215 Jefferson Davis Highway, Suite 1204, Arlington, VA 22202-4302. Respondents should be aware that notwithstanding any other provision of law, no person shall be subject to any penalty for failing to comply with a collection of information if it does not display a currently valid OMB control number.
PLEASE DO NOT RETURN YOUR FORM TO THE ABOVE ADDRESS.

1. REPORT DATE *(DD-MM-YYYY)* 25-03-2009	2. REPORT TYPE Final Report	3. DATES COVERED *(From – To)* 1 January 2006 - 28-Jan-10

4. TITLE AND SUBTITLE Electrical and mechanical behavior of nano-filled polymers through molecular dynamics simulations	5a. CONTRACT NUMBER FA8655-06-1-3009
	5b. GRANT NUMBER
	5c. PROGRAM ELEMENT NUMBER
6. AUTHOR(S) Dr. Ricardo J Simoes	5d. PROJECT NUMBER
	5d. TASK NUMBER
	5e. WORK UNIT NUMBER

7. PERFORMING ORGANIZATION NAME(S) AND ADDRESS(ES) University of Minho Department of Polymer Engineering Guimaraes 4800-058 Portugal	8. PERFORMING ORGANIZATION REPORT NUMBER N/A

9. SPONSORING/MONITORING AGENCY NAME(S) AND ADDRESS(ES) EOARD Unit 4515 BOX 14 APO AE 09421	10. SPONSOR/MONITOR'S ACRONYM(S)
	11. SPONSOR/MONITOR'S REPORT NUMBER(S) Grant 06-3009

12. DISTRIBUTION/AVAILABILITY STATEMENT

Approved for public release; distribution is unlimited.

13. SUPPLEMENTARY NOTES

14. ABSTRACT

This report results from a contract tasking University of Minho as follows: The aim of this project is to study the evolution of the nanotube network with mechanical deformation (uniaxial, biaxial) and the subsequent impact on the anisotropy of electrical and mechanical properties of these polymeric materials reinforced with nanofibers and nanotubes. Although there is a wide range of variables of interest in the case of nano-reinforced polymers, a special focus will be given to the effects of nanofiber concentration and length as well as the much less understood role of nanofiber flexibility (persistence length/rod length <1) and initial preferential orientation. This project will improve the understanding of the mechanisms responsible for changes in electrical properties during deformation of nano-reinforced polymers.

15. SUBJECT TERMS
EOARD, Polymer Materials, Nanofibers

16. SECURITY CLASSIFICATION OF:			17. LIMITATION OF ABSTRACT UL	18, NUMBER OF PAGES	19a. NAME OF RESPONSIBLE PERSON WYNN SANDERS, Maj, USAF
a. REPORT UNCLAS	b. ABSTRACT UNCLAS	c. THIS PAGE UNCLAS		59	19b. TELEPHONE NUMBER *(Include area code)* +44 (0)1895 616 007

Standard Form 298 (Rev. 8/98)
Prescribed by ANSI Std. Z39-18

Project FA8655-06-1-3009

”Electric and Mechanical behaviour of nano-filled polymers
through molecular dynamics simulations”

Final Phase II Report

Institute for Polymers and Composites - University of Minho

Ricardo J. Simoes (P. I.), Jaime Silva

March 27, 2009

Table of Contents

List of Figures

List of Symbols, Abbreviations, and Acronyms

KCL : Kirchoff Circuit Laws

KVL : Kirchoff Voltage Law

SVD : Singular Value Decomposition

GMERS : Generalized Minimal Residual Method

FMM : Fast Multipole Method

APAC : All Paths and Cycles algorithm

<k> : Average Degree

D: Fiber diameter

L: Fiber length

1. Summary

The main goal of this project is to study the electrical properties of a nanofiber network and the time-dependent evolution with mechanical deformation. In order to tackle this complex topic, we start by characterizing and representing the material system on the computer. The selected methodology employs the Graph Theory, which is a mathematical abstraction and an efficient method for analyzing paths and networks.

The first 6 months of work have been devoted to analyzing available methods and benchmarking different Graph Theory algorithms. It was concluded that no existing methodology would fulfill the specific needs of this project; therefore, new algorithms were developed as required. A preliminary study was conducted to demonstrate the usefulness of the developed algorithms.

Months 7-12 months were mostly devoted to the development of an algorithm that extracts from a Graph the Kirchoff Circuit Laws (KCL) and to the implementation of the breakdown voltage algorithm that on the next stage would enable us to calculate the electric properties of the material system. At this point, the electrical behavior at a local level could already be determined using the developed methodology, and thus the method only needed to be scaled up to extend the calculation to the entire domain.

In the first half of the second year of the project (months 13-18), the developed tool was expanded to calculate the local electrical behavior throughout the entire domain, allowing global properties to be determined. The tool was then validated through extensive testing under various conditions and for a wide range of materials. The degree of complexity and the scaling factor of the main algorithm were measured. A set of studies were conducted to evaluate the dependence of the material response on several identified nanofiber network parameters, particularly the fiber concentration and fiber length.

During the second half of the second year of the project (months 19-24), the previously ongoing studies were continued, results that had been obtained for the different metrics implemented in the previous semester were analyzed, and a set of new studies (as planned in the previous Interim Report) were started.

The third year of the project (months 25-36) focused on the effect of fiber orientation and degree of dispersion on the capacitance, effect of the clustering distribution on the permittivity, and the effect of the fiber network anisotropy on the properties. Several links were established between simulations and experiments, providing valuable validation of the simulation results.

In this third year, the paper previously submitted to Nanotechnology was published. Two other papers, already accepted in Composite Interfaces and also Journal of Nanoscience and Nanotechnology are still in press. Oral presentations were accepted in 2 upcoming international conferences: Materials 2009 and Eurofillers 2009. Currently, three other papers are being prepared.

2. Introduction

The addition of carbon nanofibers to a polymeric matrix is known to affect its mechanical and electrical properties. The changes can be significant even at small volume fractions of the reinforcement. The electrical properties are particularly sensitive to the concentration of the nanofibers, which is believed to result from the network of highly conductive nanofibers forming preferential pathways for the electrical current to flow through. The nanofiber concentration, aspect ratio, and dispersion are expected to affect the material response.

However, the precise mechanisms responsible for the described effects are not sufficiently understood. This, on one hand, is due to the complex nature of the behavior of polymers, which exhibit a complex structure and a variety of factors that influence the material behavior, such as the thermomechanical processing history, time-dependent behaviour, anisotropy, etc. On the other hand, it is also due to the inherent difficulty in analyzing the complex nano-fiber networks. Moreover, because of that complexity and a lack of understanding of the underlying phenomena, there are no adequate predictive methods that allow the creation of knowledge-based structures tailored for specific electrical response.

The Graph Theory is a mathematical abstraction and an efficient method for analyzing paths and networks. It has been widely employed to study flow in pipes, electric conduction, and even minimum travel distance problems. Results from the application of the Graph Theory were interpreted in terms of possible paths for electrical conduction. This approach considers the distance between neighboring fibers as well as their relative positions. Note that the developed methodology can be applied both to carbon nanotubes and carbon nanofibers, with adjustments to the model parameters (scale, reinforcement shape and aspect ratio, reinforcement properties, type of surface mesh generated on the reinforcement, etc).

There has been considerable amount of attention dedicated in the past few years to the reinforcement of polymers with nanoscale inorganic materials, such as carbon nanotubes, carbon nanofibers, and different types of mineral clays.

In the case of nanotubes, the diameter ranges from a couple to a few nanometers (for single-walled tubes) and have a length of a few to several micrometers. Due to their small size and high aspect ratio (from several hundreds to over a thousand), it is possible to obtain percolation at very low concentrations. The addition of carbon nanotubes produces nanocomposites with very interesting properties, both in terms of conductivity and mechanical properties. The nanotubes can improve the matrix with respect to solvent resistance, temperature resistance and thermal stability, and others. The critical issue in nanotubes is how to achieve adequate dispersion in and adequate adhesion to the matrix, without which they are of little use.

In the case of nanofibers, they typically have a diameter on the order of 10–200 nm and length on the order of several to hundreds of micrometers. In the case of nanofiber reinforcement, the issues of dispersion and adhesion to the matrix are critical, similarly to

the case of carbon nanotube reinforcement. In fact, many of the challenges in both cases are similar, especially processing, characterization and modeling.

The present work hopes to tackle those challenges and provide insights on the phenomena responsible for the electrical behavior of nano-fiber reinforced polymers through the concomitant use of simulations and experiments. This will pave the way to the future creation of knowledge-based advanced materials.

3. Methods, Assumptions, and Procedures

3.1. Overview of the method

In our approach we decided to employ a capacitor plate model (similarly to that described in [1]), but extrapolating for a 3D random array of conducting cylinders (which represent the nanofibers) and taking advantage of the capabilities of the Graph theory. By defining a cut-off radius we can build a Graph (and we have developed a methodology to allow it to be undirected) represented by an adjacency list. In our earlier work, the edges of the graph were an abstraction for the electric current. Currently we have refined the approach so that the edges of the graph represent the charge of a capacitor, and the vertices represent the plates. This enables the use of the boundary element method, to extract the capacitance of the conductors and, by using the graph theory, to extract the Kirchoff Circuit Laws (KCL). After the extraction of the KCL we solve them by SVD decomposition.

Knowing the charge in all capacitors, we can get an approximation of the electric field and we can then compare with the lower limit of the dielectric strength. If the electric field in some capacitor is greater than the lower limit, then the dielectric behaves like a conductor and the two fibers are at the same potential. This results in physical changes in the material system, requiring a new Graph to be created. We thus update the graph and perform another iteration until at least one path for conduction is formed between two exterior points (s and t). The output of this procedure includes the status of several parameters when the material starts conducting, such as the potential drop and the global change, from which the remaining quantities of interest can be calculated.

The employed procedure for prediction of the electrical properties is based on 3 main stages: creation of nanofiber-reinforced amorphous materials on the computer, analysis of the material and extraction of a Graph, solving the electrical problem (circuit laws) and calculation of the electrical properties.

3.2. Computer generated materials

We start by creating materials on the computer that capture the essential features of the real materials under study. More precisely, the computer-generated materials are comprised of an amorphous phase and the reinforcing nanofibers. We employ the statistical segment model advocated by Flory, where the amorphous phase consists of chains of linked statistical segments. This model is often labeled a coarse grain model and allows for simulations at a larger scale than those using the united-atom model or those performed at the atomistic level. Each statistical segment is positioned in 3D space within the bounding box of the simulation cell and represents several repeating units of a real macromolecular polymeric chain.

In the first step of the material generation procedure, the simulation cell boundaries are defined and the nanofillers are positioned within the enclosed 3D volume. The nanofillers are added by random sequential addition until the desired volumetric concentration has been achieved. Although the procedure can be used to place both nanofibers and/or nanoparticles, the current study only concerns nanofibers and thus the procedure will be described for that case. The length of the fibers can be fixed or vary within a specified range; in the later case, every time a new fiber is going to be added to the system, its length is randomly assigned within the allowed range.

Whenever a nanofiber is being placed, a random position is selected for the geometric center of the fiber within the enclosed 3D volume. A direction for the main fiber vector (along the fiber length) is also randomly selected. From the center point, the direction vector, and the fiber length (defined by the user), the start and end positions of the fiber are calculated. Then, possible overlap with existing fibers is determined. If there is overlap, a new position must be found. The procedure can be configured to take one of two actions:

a) a brute-force approach where a new position and new direction vectors are defined and the new placement conditions are tested for overlap, with this procedure being repeated as many times as required to find an adequate position or until a termination condition is met.

b) test overlap for minor shifts from the attempted position, namely by first testing displacements in several directions and if unsuccessful test several fiber rotations around the attempted position. If any of these overlap tests is validated (meaning, no overlaps exist with any other fiber), the new fiber is added to the system. Otherwise, a new position and rotation are randomly selected and the process is re-started until an adequate position is found or a termination condition is met.

It is also possible to pre-define a preferential direction for the fibers, which will statistically condition the values that the fiber direction vector can take, and allows creation of systems with different degrees of nanofiber orientation along a preferential axis. Once the specified nanofiber concentration is reached, the 3D volume inside the simulation bounding box is completed with the amorphous phase. A detailed explanation of the chain generation procedure has been provided elsewhere [2]. An example of a material created in this way is shown in Figure 1.
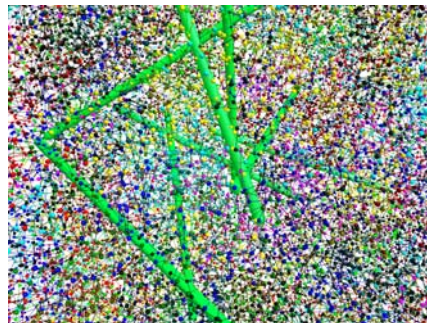
Figure 1 – Computer generated material comprised of randomly oriented nanofibers dispersed in an amorphous polymeric matrix.

3.2.1 Validation of fiber packing (random cylinder packing in 3D space)

One open question with the model in generating random cylinders is the question if the maximum concentration that can be achieved. This is a problem typically described as random cylinder packing. There are two algorithms that can be used for this purpose; one is called the sequential packing algorithm (used in this work and described in the previous section), and the other is called the collective rearrangement algorithm. The later is based in a Monte Carlo perturbation process and is believed to be able to generate tighter structures.

For relatively low concentration materials, the use of the sequential packing algorithm is appropriate, but its effectiveness for higher concentrations was an open question. To validate the process, we have used the formula proposed by [3], which is widely accepted as the general rule for the cylinder packing problem.

$$\phi = 5.4 \frac{D}{L}$$

The algorithm follows the theoretical boundaries and can be used for aspect ratios greater than 15. In order to achieve these boundaries it was necessary to change the data structure to one with a lower complexity; this was done by implementing oriented bounding box trees. With this type of data structure more cylinders can be tested for overlap in a shorter time, and it also allows for further future development (with minor changes) in the generation of arbitrarily shaped fillers that can be imported for instance from a CAD program.

3.3. Model

We start by representing the nanofibers as cylinders, the cylinders representing the charge density of the nanofiber. From the distribution of the nanofibers we build an undirected graph (abstract representation, where the edges represent the dielectric and the vertices represent the nanofibers). Using the Graph theory we can generate the Kirchoff Circuit Laws from the undirected Graph. For using the Kirchoff Circuit Laws, we need the assumption that the nanofibers are conductors [4]. If they are conductors we approximate a pair of nanofibers to a capacitor; knowing the capacitance for each pair of conductors we can introduce this parameter in the Kirchoff Circuit Laws. Finally, by continuously increasing the potential drop in small steps, and monitoring the generated paths for conduction, we can obtain the potential drop when the material starts conducting. We can describe (in a simple form) our model in six steps:

3.3.1. Building an undirected graph

The objective of this step is to extract from the initial adjacency list a connected Graph suitable for using some Graph definitions. We can then find if the initial Graph is connected. If it is connected then there is a subgraph which includes two exterior vertices

s and *t* (these two exterior vertexes are a virtual representations of the exterior potential drop). Removing from the initial adjacency list the vertices that are not contained in the subgraph, we can say that the Graph is connected and the updated adjacency list represents this Graph.

3.3.2. Extracting the capacitance for each pair of fibers

In the previous step we formed a connected graph. Now we can use Kirchoff Circuit Laws to solve the problem, using for instance the approach in [5]. For that we formulated a capacitance extraction problem. We then solve this problem for each edge in the adjacency list using the fast multipole method applied to capacitance extraction problem [6, 7, 8] to extract the capacitance matrix.

The fast multipole method is an algorithm to reduce the O(n3) order to a O(n) order, for problems that require the evaluation of all pairwise interactions in large ensembles of particles, and for solving certain partial differential equations by first recasting them as integral equations using for instance the Boundary Element Method [9]. With this matrix we can build a virtual electric circuit where the edges represent the capacitors and the vertices the plates of the capacitor.

We also add a new edge between s and t that represents the applied potential drop. This added edge is necessary for forming a set of electric circuit equations with an unique solution. Then we can apply some linear algebra methods to the graph and extract the Kirchoff Circuit Laws.

3.3.3. Extracting the Kirchoff Circuit Laws

In our undirected graph the edges represent the capacitor and the vertices the plates of the capacitor; we have only capacitors in our circuit and one edge representing a potential drop. So far we have a way of finding the capacitance of each capacitor (fiber pair), outlined in the previous step. Now we can use one of following methods to extract the Kirchoff Circuits Laws: Linear algebra method: First we convert the adjacency list to a directed incidence matrix, and then we solve the linear system $Bx = 0$ where the output are the null vectors or the Kirchoff Voltage Law.

Modified APAC: With a modification in the APAC algorithm we can get all the independent simple cycles of the Graph or the Kirchoff Voltage Law.

From the incidence matrix we get n independent Kirchoff Current Law equations and from one of the previous methods we get m independent Kirchoff Voltage Law equations.

3.3.4. Calculating the charge in each edge (capacitor)

From the previous steps we build a square matrix with Kirchoff Circuits Laws. We can now form a linear system and solve it by SVD decomposition for some potential drop. At the end of this procedure we know the charge Q_i in each edge.

3.3.5. Finding the potential drop for each edge

This is a simple procedure, where we solve the capacitor equation to get the potential drop in each edge and compare it with the dielectric strength.

3.3.6. Iterate the process until a path for conduction is created

From the previous step we know when the local dielectric breakdown occurs and for each such event we update the Graph and perform another iteration. By updating the Graph, we mean removing the capacitors that have an electric field greater than dielectric strength and substitute them by a thin conductor with no resistance in the circuit.

3.4. Physical Model

To simulate this complex N-body problem, we decided to apply the capacitor plate model [1], but extrapolating for a 3D random array of conducting cylinders and using the Graph Theory. In our model the nanofibers are conductors [4], randomly dispersed in an isotropic homogeneous dielectric matrix. A Graph is built to represent the nanofiber network. The Graph edges represent the charge of a local capacitor, the nodes are the conductors (plates of the local capacitor), and the edges that contain the virtual nodes, source (s) or sink (t), represent a perfect conductor. These local capacitors only have two states, charged and uncharged. The sink (t) and the source(s) are connected to a potential drop that we increase in small steps, until by discharging the small capacitors (starts conducting by dielectric breakdown) at least one path for conducting is formed. We assume that two nanofibers at a distance smaller than the specified cut-off radius interact with each other. We also assume the nanofibers connected to s or t share the same potential. To solve this problem, we need to find the solution only at the surfaces of the conductors, for example, by applying the boundary element method. In order to make this approach suitable to large systems, we formulated the problem for a small system (two fibres) and then extrapolate to a larger one.

In our model we assume that the only way for the capacitors to discharge is by dielectric breakdown [1, 10, 11]. To simulate capacitor discharge, we continuously increase the voltage between the virtual nodes until a point is reached where the dielectric is not capable of sustaining any further voltage increase. This will result in the formation of a permanent conductive channel between the two conductors. In this way, the breakdown procedure is done locally. The dielectric breakdown occurs first in a pair of conductors; the global domain starts conducting when one (or more) path for conduction is created between the virtual nodes. Thus, by applying a potential drop to s t in small steps, and looking for the local electric field strength (between two conductors), we can determine if a conduction path has been created. The method used to find the local electric field is to formulate a capacitance extraction problem between two cylinders and solving the electric problem using the Kirchoff Circuit Laws, this for each increment in the potential drop.

3.5. Breakdown Voltage Algorithm

In the previous section we describe a method for extracting the capacitance matrix from n conductors in free space. This can be done in nm flops, for n conductors and m panels, using generalized minimal residual method (GMERS) and the fast multipole method (FMM) outlined in [6, 7, 8]. With the prospect of studying regions with thousands of fibers, we do not start by directly applying the procedure to the entire domain, but we restrict it - as a first approach - to the problem of two conductors in free space. This algorithm gives a better sensitivity of the physics problem than a direct application to the entire region, which would not allow us to pinpoint possible errors or limitations of the method. Knowing the capacitance for each edge of the graph we then apply graph algorithms to determine global properties.

3.6. Complex networks metrics

In order to study the effects of clustering of the nanofiber network, a new set of tools had to be developed. Our efforts in coupling the Graph theory with the electroquastatic approximation were made with the purpose of employing complex networks approaches/methods. With this in mind, we implemented two metrics based on complex networks.

The first one is based on the maximum common subgraph (mcs). This metric was proposed by Horst and Kim [12] as follows:

The distance of two non-empty graphs G_1, G_2 is defined as:

$$d(G_1, G_2) = 1 - \frac{|V(mcs(G_1, G_2)|}{max(|V(G_1)|, |V(G_2)|)}$$

Where mcs is defined as the maximal common subgraph of two graphs, and $|V(G)|$ is the number of nodes of the graph G.

Using this metric, we can find the distance between two graphs, or the degree of isomorphism (the lower the distance, the more isomorphic the graphs are) between the two graphs. We applied this metric to answer a pertinent and unsolved question in the field of electrical properties of nanocomposite materials: whether the dielectric breakdown follows the minimum distance between the fillers. We present in the discussion section the results of the application of this metric.

Still in the context of complex network analysis, a measure was implemented with the objective of knowing the network topology, called the clustering or network transitivity. Transitivity or clustering, measures the sensitivity of the network to the presence of triangles in the network. In other words it gives the probability of a vertex A being connected to a vertex C. In the language of social networks, the friend of your friend is also likely to be your friend [13].

Clustering is defined as:

$$C_i = \frac{\text{number of triangles connected to vertex } i}{\text{number of triples centered on vertex } i}$$

$$C = \frac{1}{n} \sum_i C_i$$

With this measure C_i and with k_i, we can construct a joint distribution function and find a relation to the study of permittivity. In the physical sense, clustering gives the ratio of parallel/series connections for a given node.

4. Results and Discussion

An example of a nanofiber network, created by the procedure previously described, is represented in Figure 2. The nanofibers are individual cylinders, defined by their diameter and the 3D coordinates of the two extremities. This specific system was created with random orientation of the fibers.
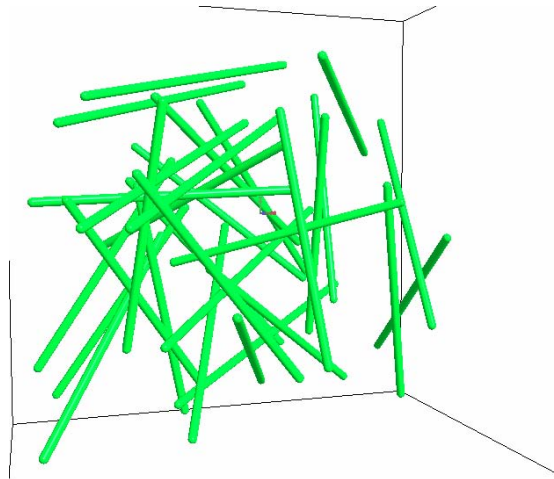

Figure 2 – Visualization of the 3D random nanofiber network.

The Graph that represents this network is shown in Figure 3 (left side). As previously described, this is the Graph that results from the minimum value of the critical radius that still results in a "connected Graph".
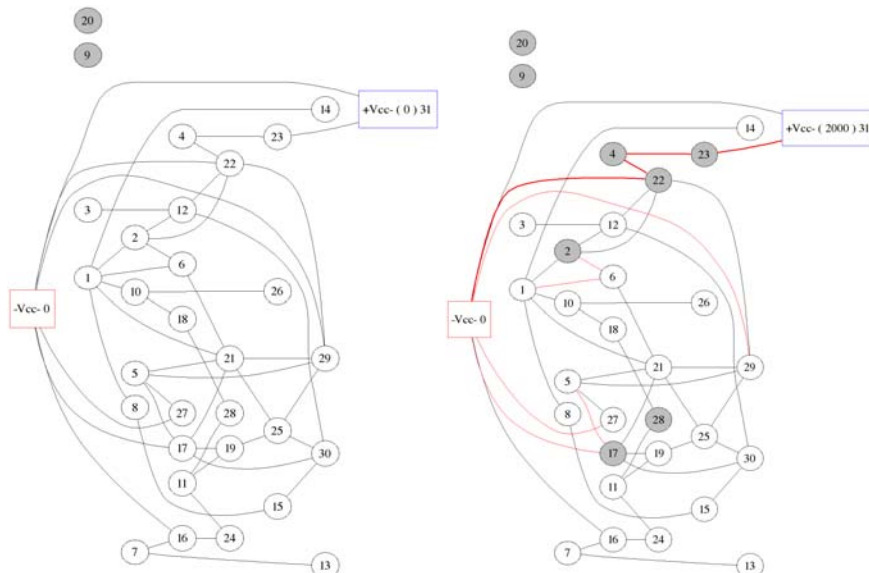

Figure 3 – Graph representation of the nanofibers (left). Representation of the conduction path (right).

Also in Figure 3 (right side) is shown the result of the application of our dielectric breakdown evaluation method to the Graph as an external voltage is applied. There are obviously many intermediate steps between the Graph on the left side and the Graph on the right side in this figure, but the right side Graph corresponds to the instant of dielectric breakdown, with a conductive path between the source and sink. This conductive path is shown as a thicker line in red.

In this figure, the nodes in gray are nodes that do not accumulate charge since there was dielectric breakdown to another node. Effectively, these nodes could be removed from the Graph, but they are shown for perspicuity sake. As can be seen in this figure, breakdown occurred at several locations, with one set of edges resulting in an effective path (nodes *s*-22-4-23-*t*). In other systems, several paths may be simultaneously created at a certain voltage step. Meaning, there will usually be several conductive paths after the application of the method, rather than a single path.

The set of parameters used in the simulations performed to validate the method and also to study the effects of fiber concentration and fiber length are shown in Table 1.

Table 1 – Material parameters for the plan of simulations performed thus far.

Simulation cell size	Level 1	Level 2	Level 3	Level 4
Length	20	40	40	50
Height	20	40	40	50
Depth	10	20	30	30

Fiber length	Level 1	Level 2	Level 3
	5	10	20

Fiber concentration (%)	Level 1	Level 2	Level 3	Level 4
	0.65	1.2	2.5	5.3

Results from this plan of simulations are shown in Figures 4-12. In Figures 4-6 are the preliminary studies for validation of the method with respect to generating a Graph and identification of possible paths for conduction. A study on the complexity of the nanofiber networks is shown in Figure 7. Typical outputs of the developed procedure for evaluation of the electrical breakdown mechanism are shown in Figure 8. The studies of the effect of fiber concentration and fiber length are in Figures 9-12.
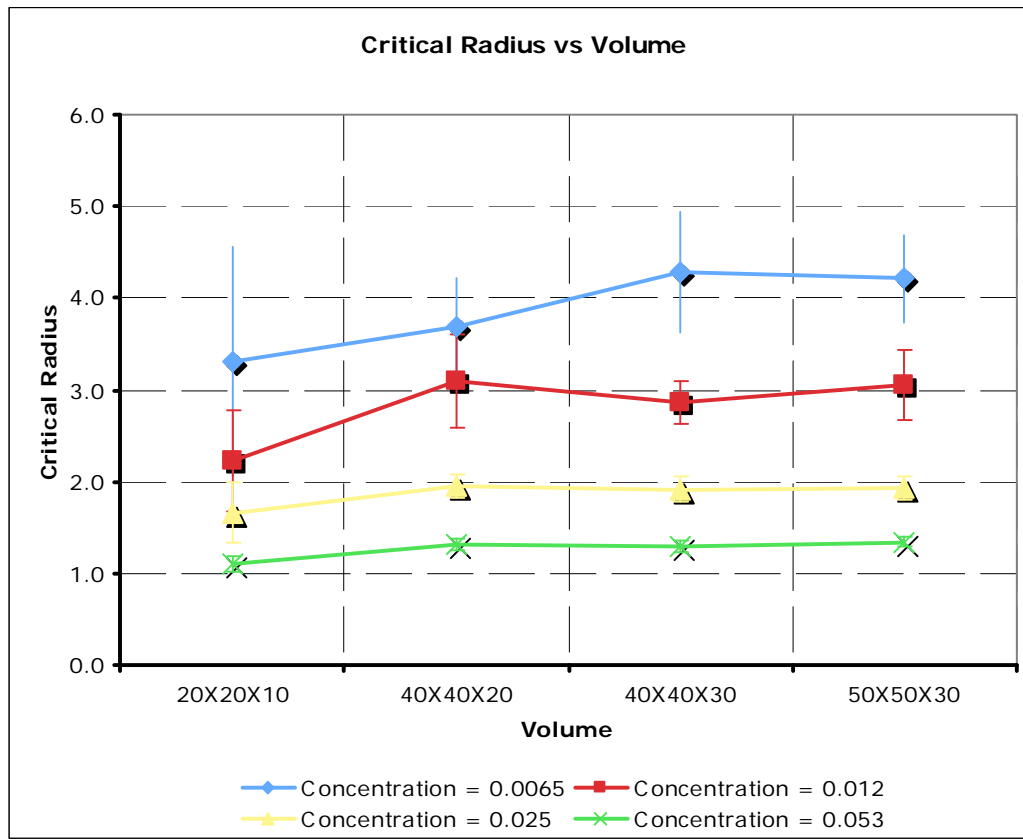
Figure 4 – Effect of the system volume and fiber concentration on the critical radius.

As can be seen in Figure 4, there is a dependency of the critical radius on the concentration, characterized by a decrease of the critical radius with an increase in concentration. This trend is similar for all volumes tested, meaning that the simulation cell size does not affect significantly the behavior of the material.
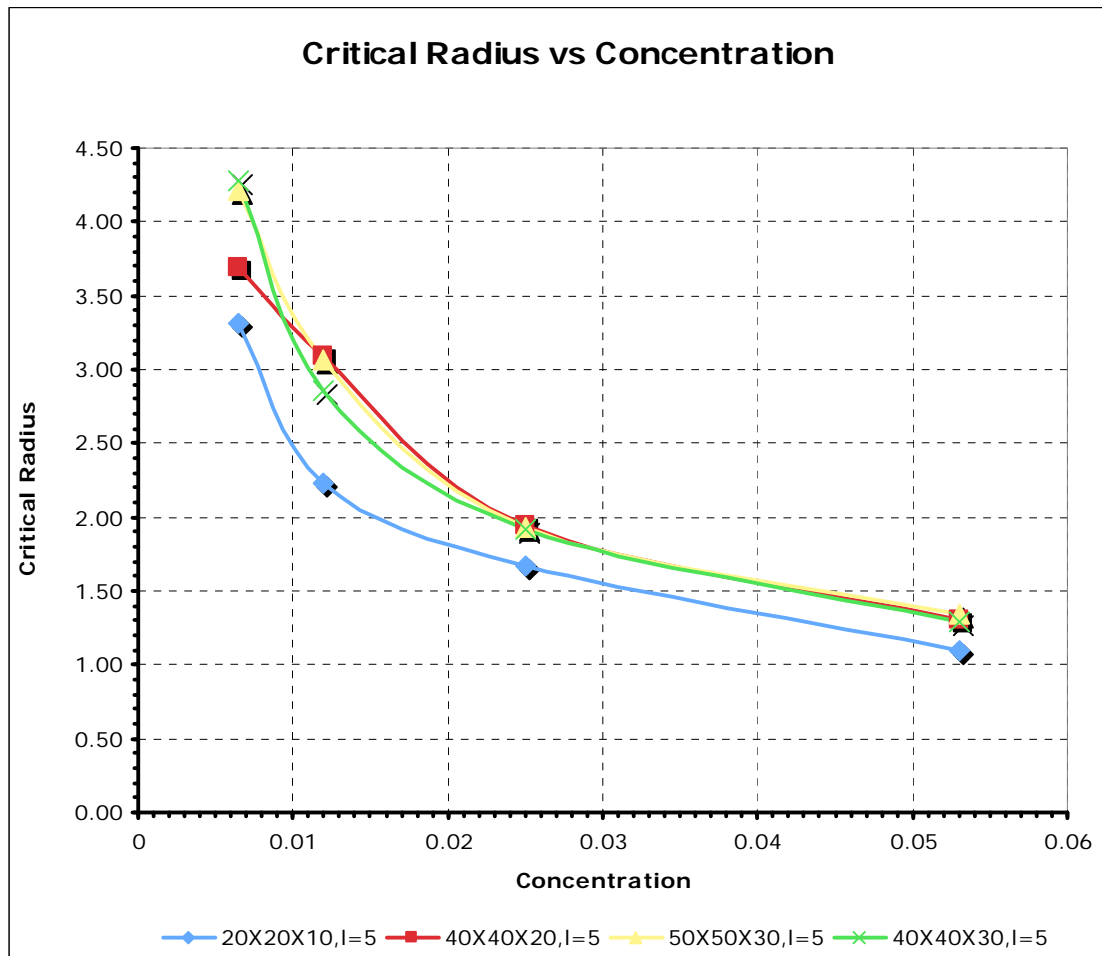
Figure 5 – Effect of the fiber concentration and system volume on the critical radius.

The information shown on Figures 4 and 5 is analogous. The effect of concentration that has been shown in Figure 4 can be seen more clearly in Figure 5, where a significant decrease of the critical radius is observed with an increase in concentration. This effect is stronger for lower concentrations, as we are further from percolation. Again here we can see that the trends are similar for all simulation volumes tested.

In Figure 6, aside from the effect of the concentration, we can see the effect of fiber length on the critical radius. It is clear that the increase of fiber length decreases the critical radius required to define a Graph for a particular network. At a fixed concentration level, even though the use of longer fibers implies there are fewer fibers in the network, the longer fibers exhibit more proximity points, making it easier to establish paths, and resulting in a decrease of the critical radius.
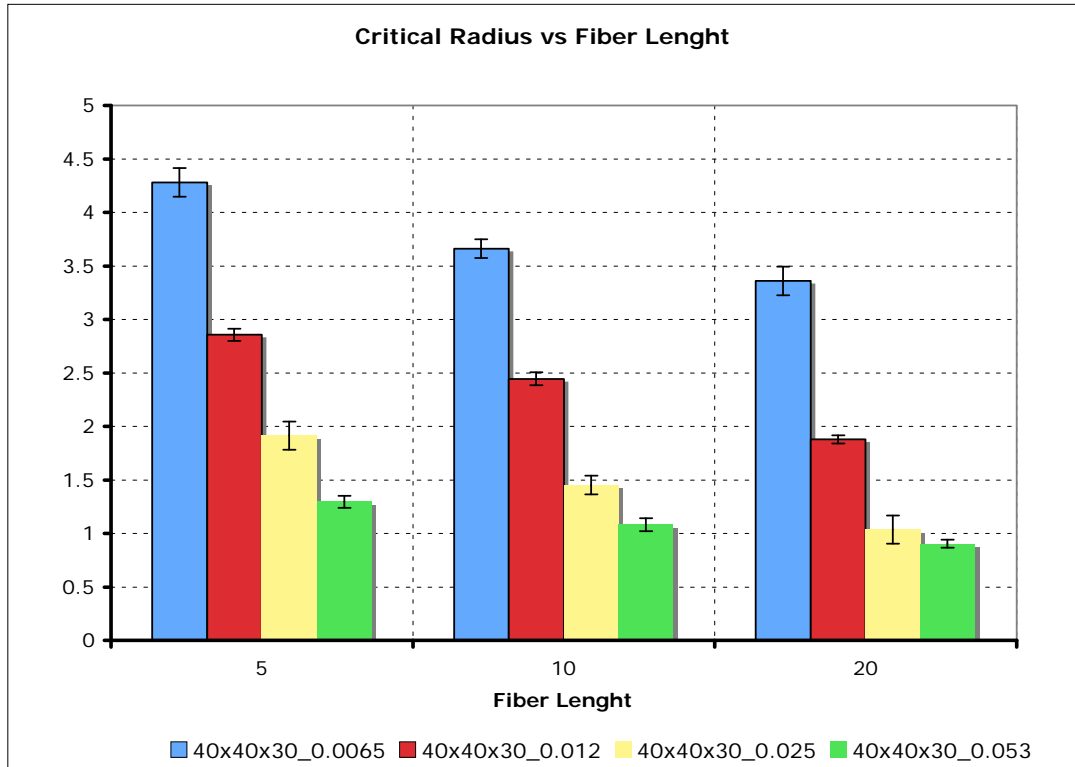
Figure 6 – Effect of the fiber length and fiber concentration on the critical radius.

In Figure 7 we represent a complexity indicator, the average degree, <k>, which is essentially a measure of the average number of first order neighbors. This parameter is calculated as:

$$\langle k \rangle = \frac{\sum\limits_{i \in V(G)} \sum\limits_{j \in E_i(G)} a_{ij}}{\max(V(G))}$$

The value of <k> is shown for several systems both immediately before breakdown and immediately after breakdown, meaning, when a conduction path was established through the material. The large differences between <k> for pre-breakdown and after-breakdown result from the fact that, after breakdown, we only consider a sub-Graph (containing only the part of the network that is involved in the conduction process) of the original Graph. We can see that the average number of first order neighbors decreases with increasing concentration.

At low concentrations, it is more likely to find that the random placement of the fibers creates disparities among different regions. Thus, there may be regions where fibers have many neighbors and others where fibers are more spread apart. This implies that to form a connected Graph throughout the material, with at least 1 possible path for conduction, we need to use a larger critical radius. That larger critical radius means an excessive number of neighbors in the regions where fibers are closer together, contributing to an

overall higher value of the average number of first order neighbors. For higher concentrations, even though there are many more fibers, <k> decreases significantly. This results from the fact that it is less likely to find regions that have sparse fiber distributions, and thus the average number of first order neighbors is smaller.
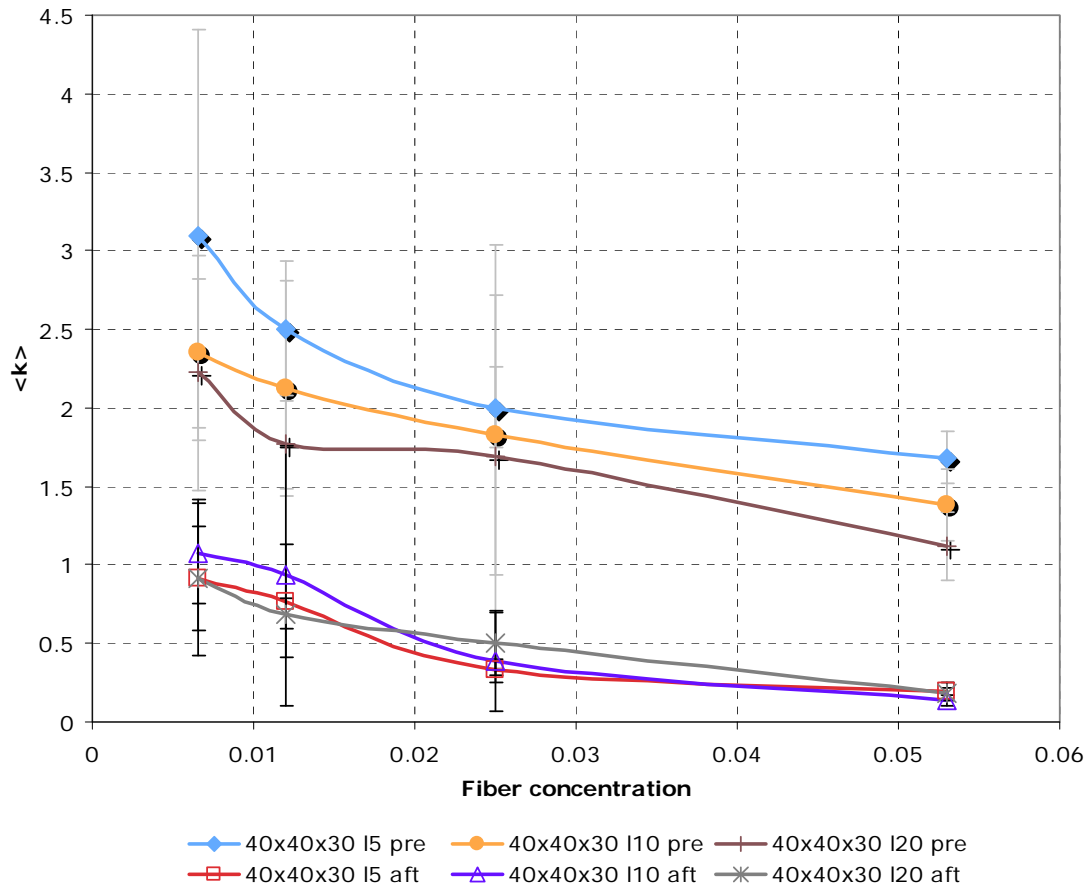
Figure 7 – Complexity of the systems, quantified by the average degree <k>.

In Figure 8 we see how the increase of external applied voltage affects the charge in the material. As we consider pairs of fibers as capacitors, this corresponds to charging the capacitors. Local breakdown will cause capacitors to disappear from the system, resulting in the discontinuities in the curves. Individual breakdowns are hardly noticeable, whereas cascade breakdown effects result in large jumps in the global charge. The increase of charge upon removal of capacitors can be seen as an increase of dielectric volume.
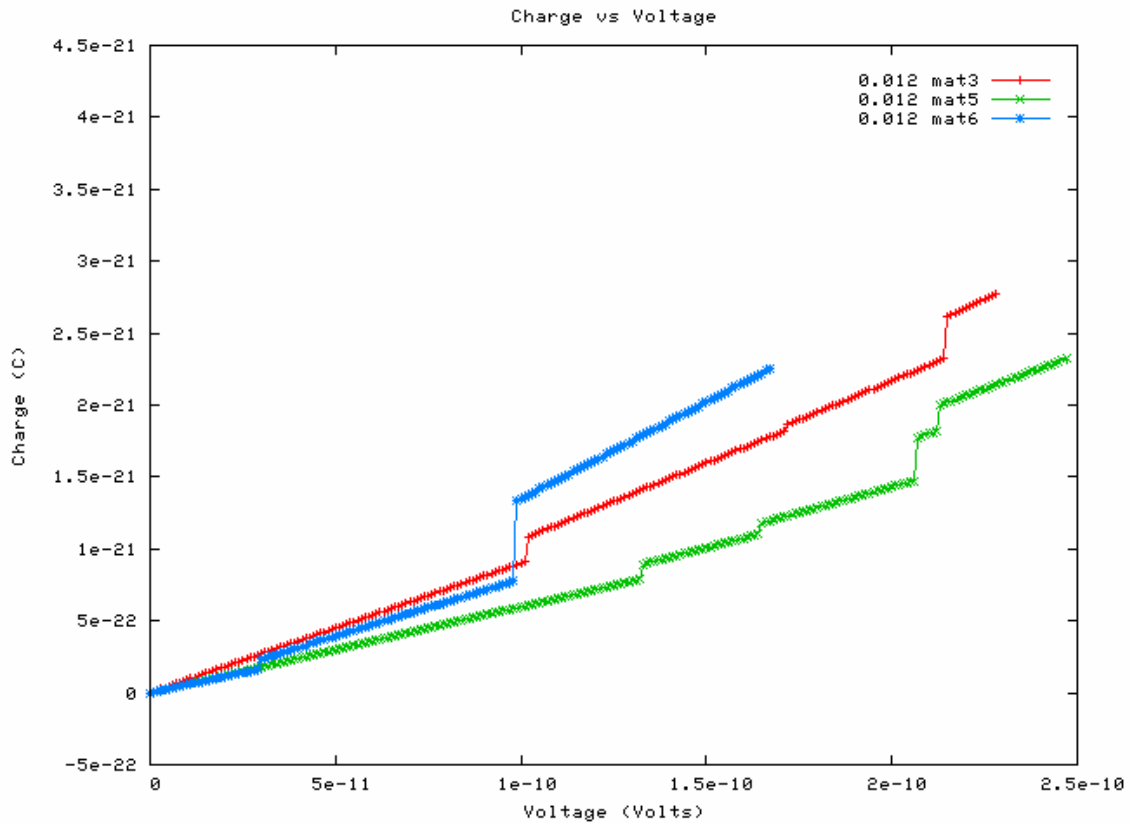
Figure 8 – Typical output of a simulation with an external applied voltage increasing up to electrical breakdown.

The maximum values of the charge and voltage immediately before breakdown were calculated for a set of simulations performed with the plan of parameters shown in Table 1, namely the fiber concentration and fiber length. For each condition, 6 materials were created with the exact same material parameters. Each value represented in Figures 9 to 12 thus corresponds to the average of the 6 materials for that condition, and the vertical error bars correspond to the respective standard deviation.

We can see in Figure 9 that the increase of concentration leads to a global decrease of the charge. When we increase the concentration we are increasing the number of conductors (fibers). As was seen before, this actually results in a decrease of the number of first order neighbors. Thus, the number of capacitors that are connected in series will increase comparatively to those in parallel.
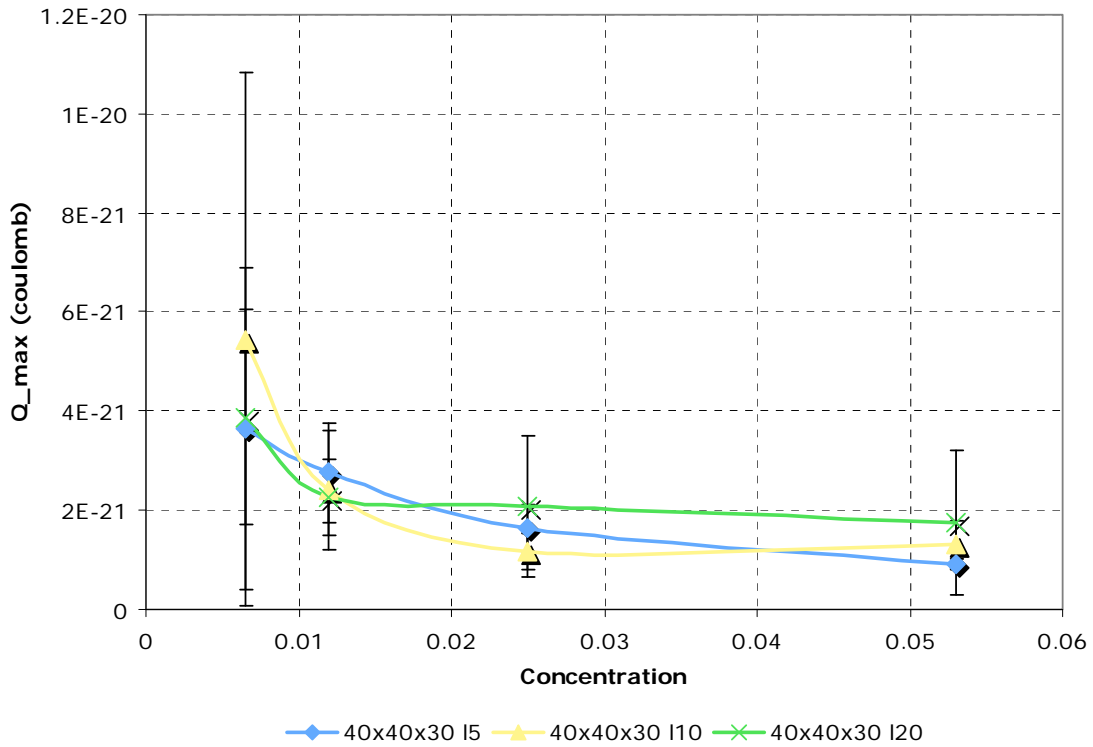
Figure 9 – Effect of the fiber concentration and fiber length on the maximum charge in the system immediately before breakdown.

It is important to notice in Figure 9 the large error bars associated with the smaller concentrations. This results from the high dependence on the specific network geometric arrangement for lower concentrations. Because of this, the influence of the length of the fibers is difficult to establish. A larger number of simulations might help decrease the variability of the results.

In Figure 10 we see the breakdown voltage values, and the tendency for a decrease of the breakdown voltage with concentration. This was expected, since more conductors, and a higher likelihood of establishing paths, should result in a decreased voltage value required for inducing conduction across the material. Clearly, longer fibers also reduce the breakdown voltage, meaning, they make it easier to establish conduction paths.
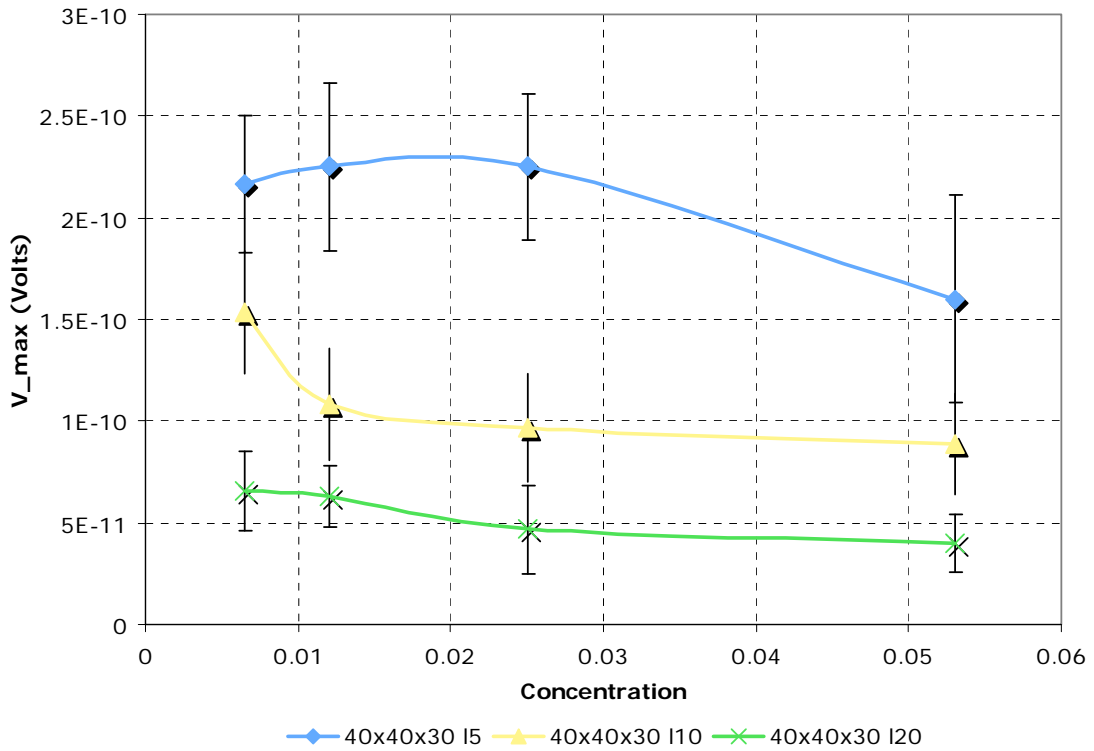
Figure 10 – Effect of the fiber concentration and fiber length on the maximum voltage applied immediately before breakdown.

The capacitance is calculated from Q = C * V, and so the values in Figure 11 are calculated from those in Figures 9 and 10. The high standard deviations again make it difficult to establish trends, but the capacitance seems to increase with increased fiber length, due to the pronounced effect of this parameter on the breakdown voltage.
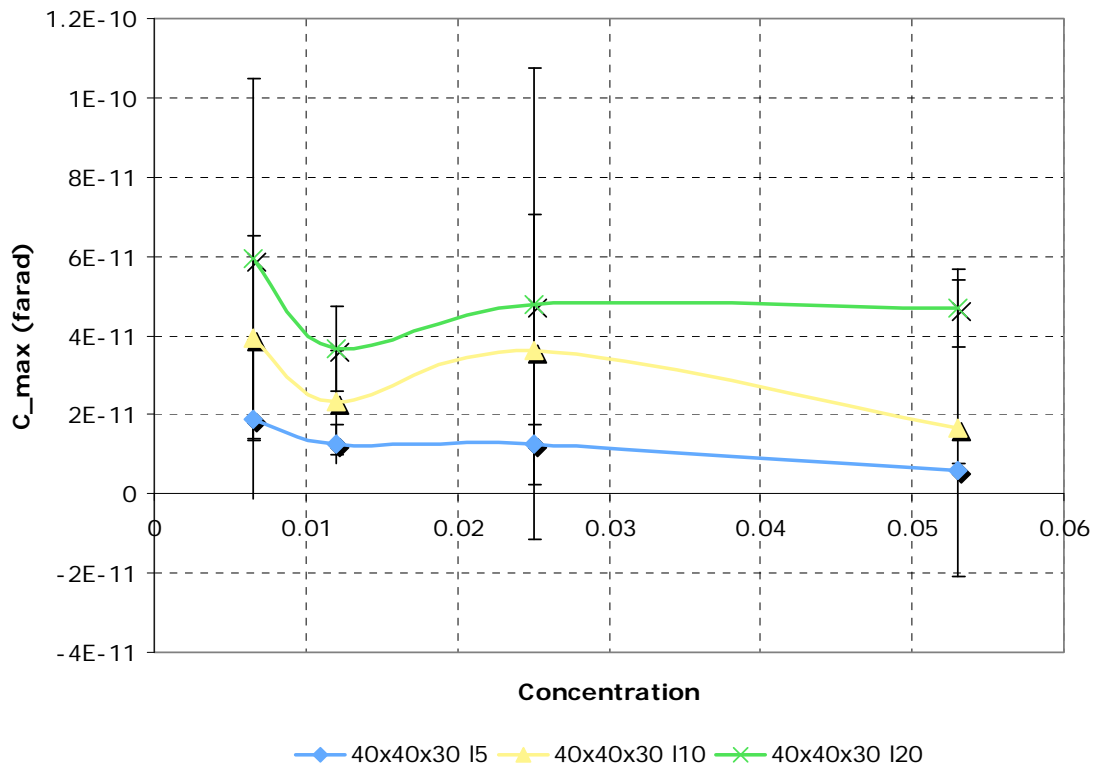
Figure 11 – Effect of the fiber concentration and fiber length on the maximum capacitance of the system immediately before breakdown.

The relative permittivity, shown in Figure 12, is calculated approximating the simulation cell to a parallel plate capacitor with a dielectric medium. We can find for the dielectric without the nanofiber network that C_init = ε_init * (Area / distance). Since we know C_max for the final configuration, which now contains the nanofiber network, we can then apply (C_max / C_init = εr / ε _init) and obtain εr. The permittivity does not exhibit a clear dependency on the concentration, but it increases for increased fiber length. This effect is obviously related to the dependency previously seen in Figure 11 for the capacitance, since we obtain the permittivity from the capacitance.
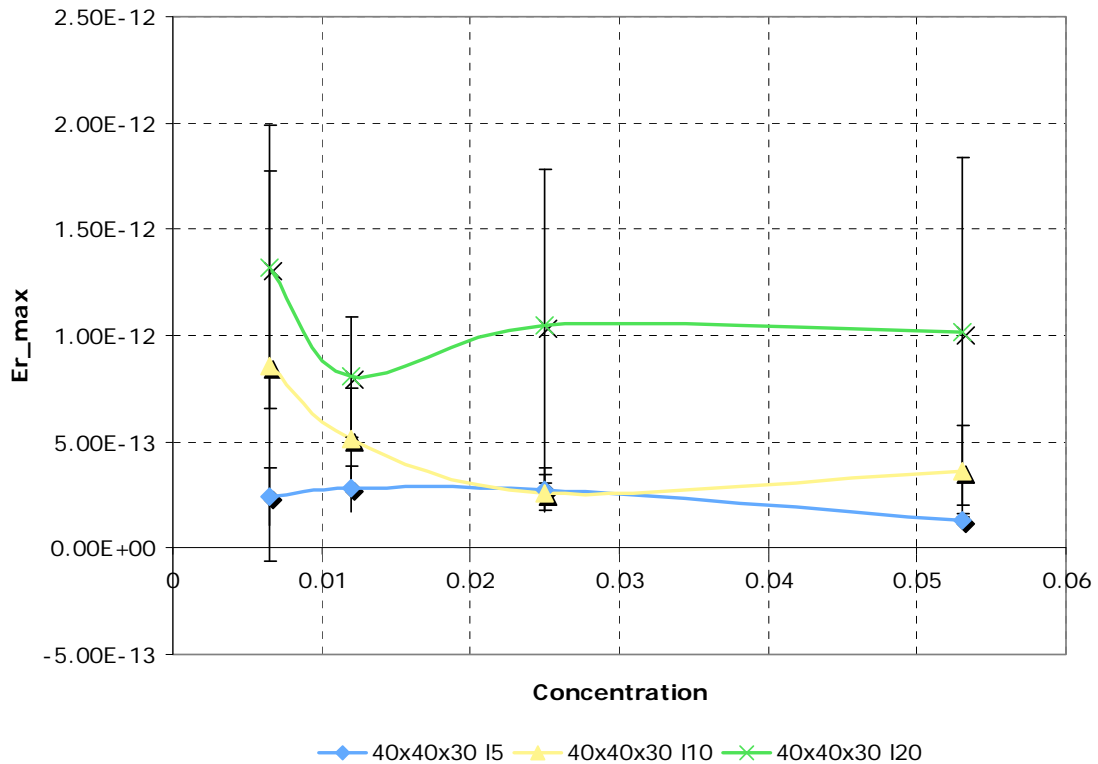
Figure 12 – Effect of the fiber concentration and fiber length on the relative permittivity of the system immediately before breakdown.

Effect of the fiber orientation and average distance on the capacitance

The effects of the relative orientation of fibers and the distance between them on the capacitance are important aspects when trying to establish structure-properties relationships that consider the nanofiber network spatial arrangement. To this end, we have made iterative changes in relative orientation and distance between pairs of nanofibers. Figure 13 shows schematically how the fiber position changes when they are displaced with respect to each other, either perpendicularly to their main axis (x axis) or along their main axis (z axis). Note that one fiber is fixed in 3D space and another single fiber is used for each measurement.
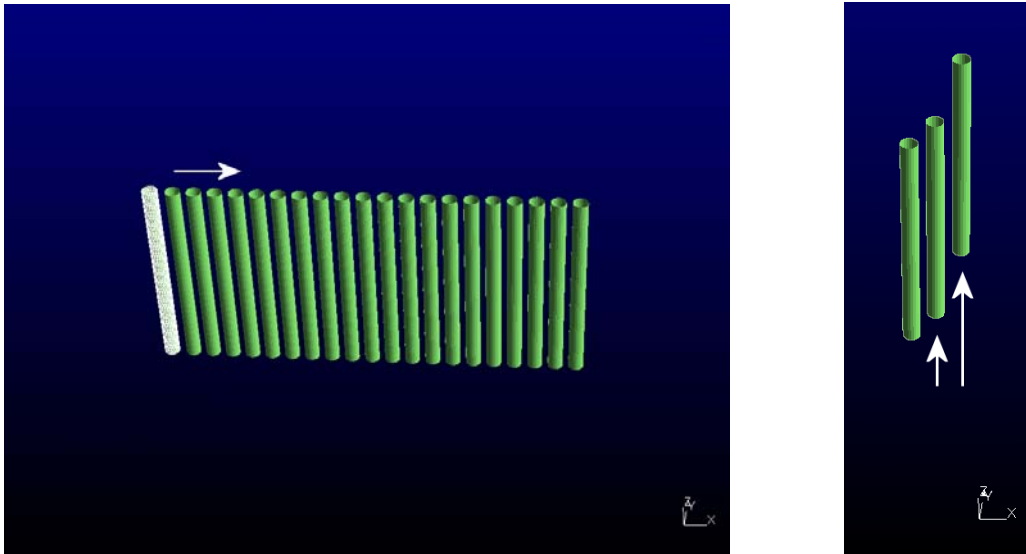
Figure 13 – Relative displacement of fibers along X (Trans_XX) or along Z (Trans_ZZ). Note that in the figures multiple fibers are shown for visualization purposes only. The capacitance calculation is performed with only a pair of fibers, one being fixed and the other displaced iteratively.

The results for the capacitance with increased separation are shown in Figure 14. As could be expected, the capacitance decreases with the distance. It is useful to make here an analogy to parallel plates, where the capacity is directly proportional to the area of the plates and inversely proportional to the distance between plates.

For the case of increased distance between the main axis of two parallel fibers (Trans_XX), the capacitance decreases as a function of 1/d (initial steep decrease with increased distance and then smoother decrease tending towards a plateau around 50-60nm distance). However, in the case of increased distance when a fiber is displaced along its main axis (Trans_ZZ), there is a linear decrease of the capacitance with distance while a part of the two fibers are still in close contact up to roughly 20nm (note that a 10nm displacement means that only half of the fibers are now in close contact, since the fibers have a length of 20nm). After 20nm, the decrease is smoother and then after 30nm the values become similar to those observed for similar distances in Trans_XX. The linear decrease of the capacitance for small Trans_ZZ distances is related to the amount of contact surface area, which is decreasing linearly while the two fibers are displaced relatively to each other.
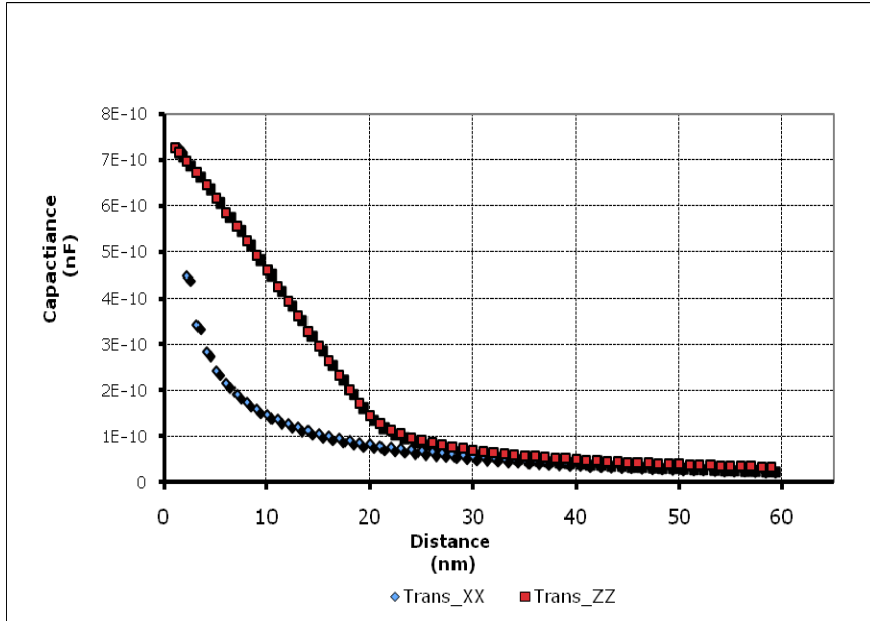
Figure 14 – Effect of the distance between two fibers on the capacitance.

Figure 15 shows schematically the study of the relative orientation between fibers. For this study, a fiber is maintained fixed in 3D space and another is rotated about an axis. Note that in the first case (Ry), the minimum distance between the two fibers depends on the rotation angle. In the second case (Rx), the minimum distance between the two fibers is constant, but the amount of surface area that is at the minimum distance varies with the rotation angle.
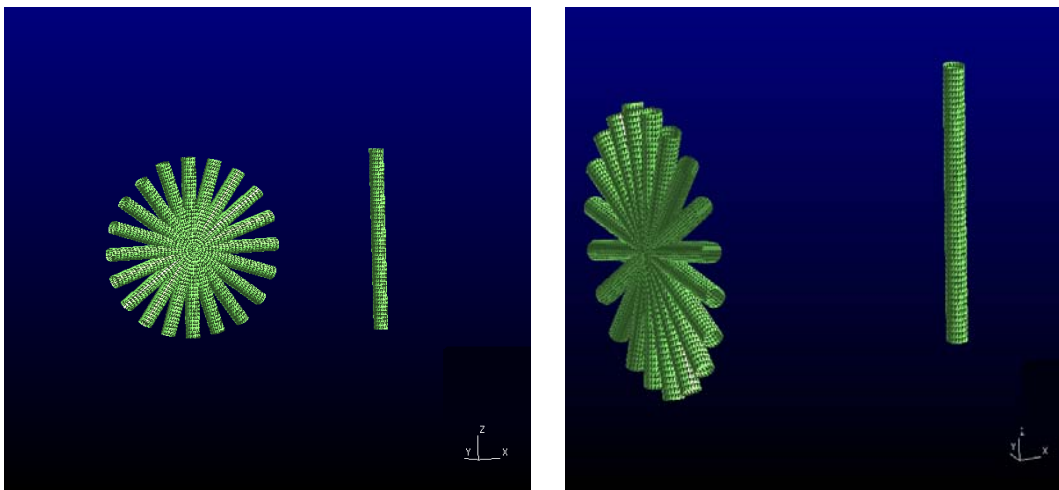
Figure 15 – Relative orientation of fibers about the y axis (Ry) or about the x axis (Rx). Note that in the figures multiple fibers are shown for visualization purposes only. The capacitance calculation is performed with only a pair of fibers, one being fixed and the other displaced iteratively.

The results for the capacitance with increased separation are shown in Figure 16. There is a significant influence of the rotation of the fiber about the y axis, since the distance between fibers decreases considerably, in fact up to half the original distance at 90º and 270º rotation angles (even though the surface area that is at the minimum distance at these angles is much smaller than at 0º and 180º). However, the capacitance is not significantly affected by rotation about the x axis, even at a 90º rotation angle, which is quite interesting. This implies that in practical terms, the distance has a much stronger effect than the rotation angle.

This occurs because even at large rotations of one fiber about the x axis, even though only the center region of the two fibers are at the minimum distance between them, the distance between any other points on the surface of the two fibers is not significantly different.
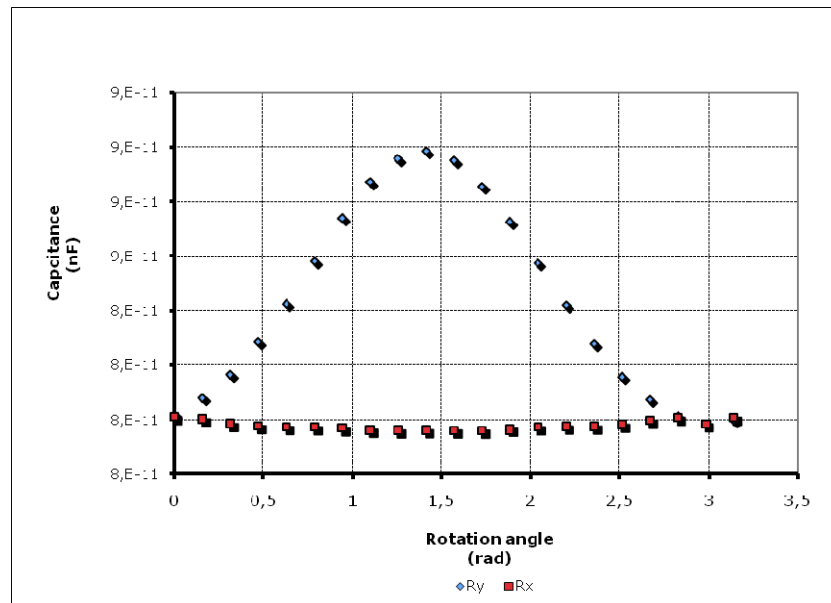
Figure 16 – Effect of the angle between two fibers on the capacitance.

Effect of local clustering distribution and its relation to the permittivity

To study the effect of fiber clustering, we generate different network arrangements for a concentration of 0.0065 in a 4000x4000x3000 nm^3 volume with random distribution of fibers with an aspect ratio of 5 and fixed critical radius. We then employ boxplots to represent the relationship between clustering values and permittivity. The results are shown in Figure 17.

The boxplot is a powerful way of displaying results without any statistic assumptions. The boxplots are constructed by the calculation of the lower quartile, upper quartile and the interquartile range (IQR) ,which is the distance between the upper and lower quartiles. The dotted lines called inner fences and outer fences represent 1.5*IQR below the lower quartile and 3*IQR above the upper quartile. The values that fall between the inner and outer fences are called outliners. The values that fall outside the outer fences are called highly suspected outliners. Outliners in this case represent a rare event; the effect of these events are discussed later.
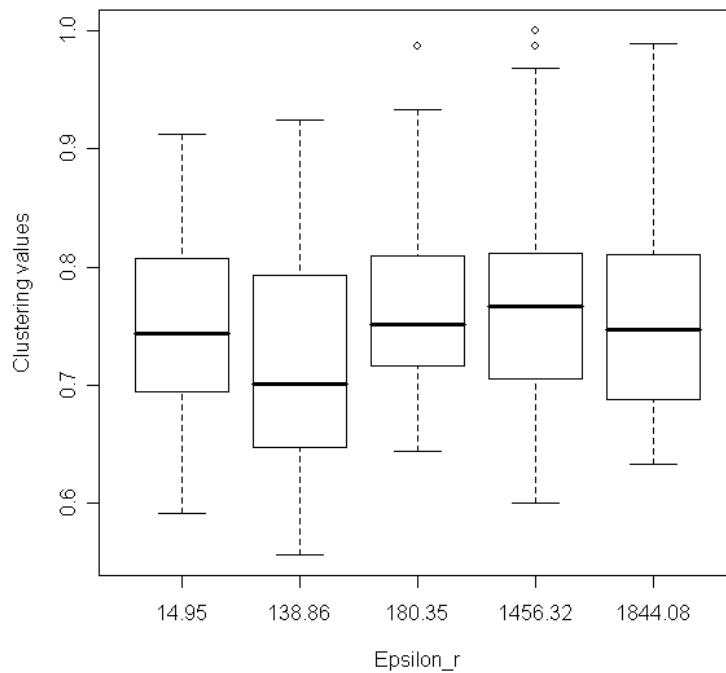
Figure 17 – Boxplots for the local clustering distribution in 5 materials and their permittivity.

It can be seen from Figure 17 that the permittivity is greater in the presence of higher number of fibers with large values of clustering. Thus, a small number of vertices with higher clustering values results in a stronger contribution to the permittivity.

The later statement can be verified with the joint distribution function. This function provides the probability associated with each possible value of k_i (degree) and C_i (clustering). This is shown in Figure 18 for the materials with permittivity 138.86 and 14.95 respectively.
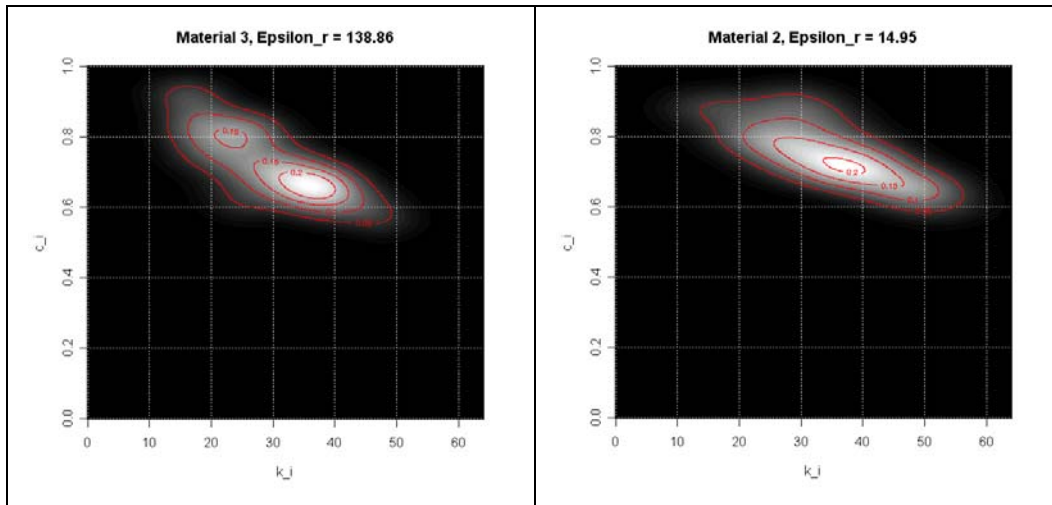
Figure 18 – Joint distribution function for the materials with permittivity 138.86 (left) and 14.95 (right).

Material 3 clearly displays two distinct points with the same probability, where in material 2 this does not occur. In material 3 the presence of these two points with the same probability is related with the occurrence of two groups (clusters) in the nanocomposite. Thus, when clustering occurs, it influences the permittivity to higher values.

This study also shows that the general approach developed so far provides a good framework in the analysis of structure-properties relationships in nanocomposites materials.

Permittivity tensor for the study of anisotropic nanocomposite materials

Until now we had focused on the case of random fiber networks, as that shown in Figure 19, as these provide a multitude of cases and parameters for study. However, it is also extremely important to characterize the case of aligned networks, which can result from processing or from the application of external fields (electric, magnetic). Our first attempt at a study of the effect of fiber network anisotropy on the properties will consider only the extreme cases: fibers aligned perpendicularly to the two plates and fibers aligned parallel to the two plates; see Figure 20.
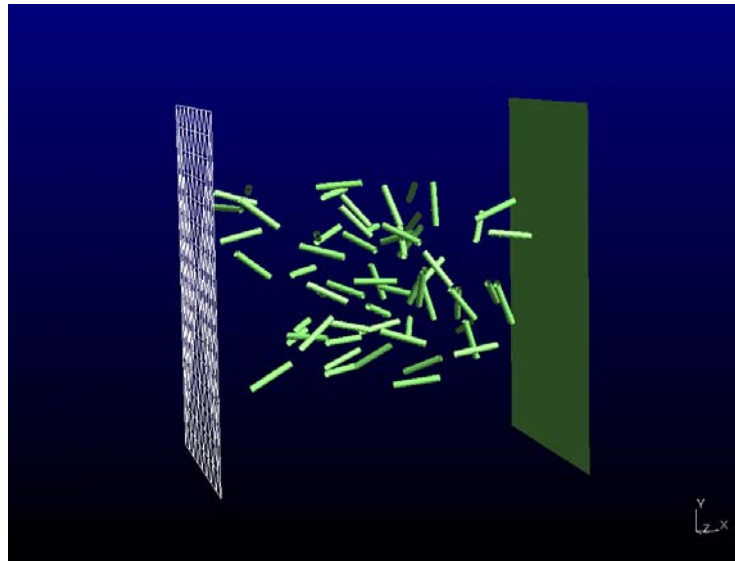
Figure 19 – Sample material with random orientation of the nanofiber network.
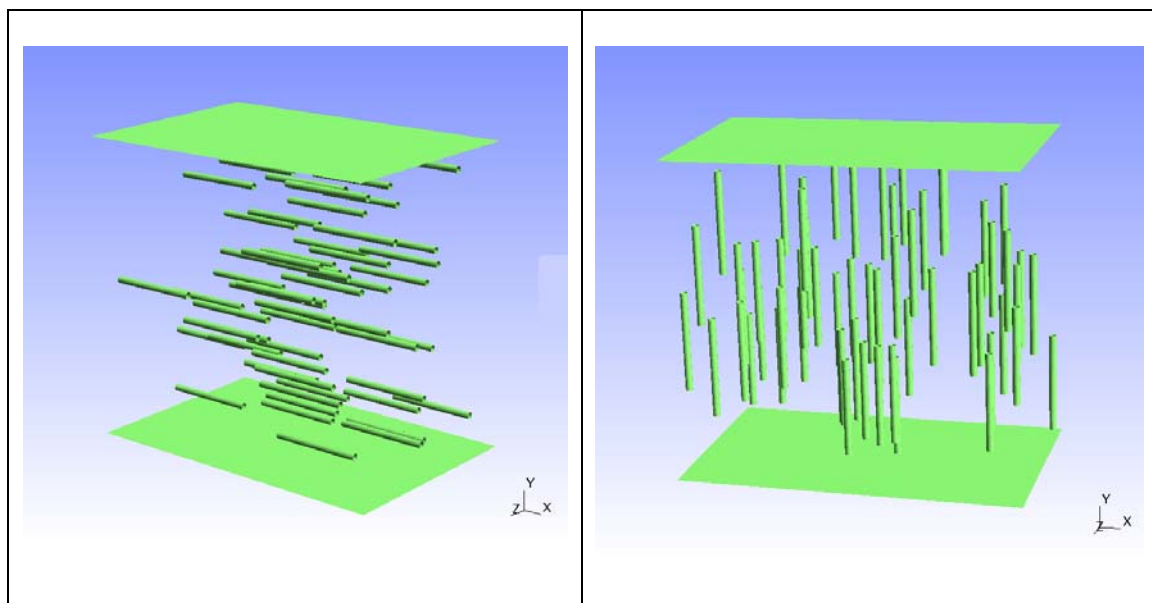
Figure 20 – Limiting cases for anisotropic nanofiber networks: fibers aligned parallel to the plates (left) and perpendicular to the plates (right).

In practical terms, the objective of this study is to characterize the diagonal of the permittivity tensor for the specific arrangements considered: random orientation, all fibers oriented in the x direction, and all fibers oriented in the y direction. Table 2 describes the parameters used for the fibers in this study. For each of the three conditions, the permittivity was calculated in the zx, zy and xy plane. This was made by changing the plates orientation for the prescribe plane calculation.

Table 2 – Material parameters for the study of fiber network anisotropy.

Concentration	0.025
Volume	48 µm^3
Fiber length	1 µm
Radius	73,21 nm

In the analysis of the results we use the boxplot method described above, as shown in Figure 21.
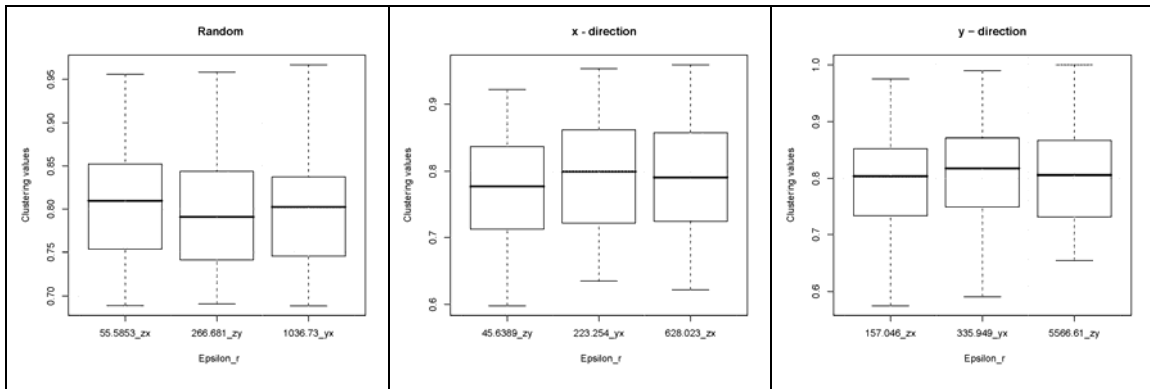
Figure 21 – Boxplots for the local clustering distribution in the 3 network arrangements under study and their permittivity.

From Figure 21 we can see that the permittivity is higher for measurements made perpendicularly to the fiber orientation. This is a strong step in the validation of the model, because intuitively we can see that a large surface is related with a large capacitance, and so the polarization of the material will be higher resulting in a higher permittivity. If the fibers are oriented perpendicularly to the input electric field, then the nanocomposite displays a large permittivity.

The material with randomly oriented fibers does not show this higher permittivity in any specific direction. In fact, the values of permittivity in this randomly orientated network arrangement are not very different from those obtained for the material with fibers oriented in the x direction.

This study also validates the later assumption made in the relation between clustering and permittivity; the clustering value for oriented fibers is only related to the minimum distance between the fibers, because they are all parallel with each other. When they are positioned in random orientations, then two adjacent fibers will rarely be aligned. The only way that high clustering nodes can be achieved is by reducing the average distance between fibers.

This type of anisotropy can be explored for future sensor applications. At this moment we are conducting more trials to validate the later results, and calculating additional properties (dielectric breakdown strength, conductivity before breakdown, etc) for these network arrangements.

Breakdown path formation mechanism

The main problem in adding conductive filler to a dielectric matrix, with the objective of increasing the permittivity, is the lowering of the dielectric strength. To study this undesirable side effect we incorporated in our model a breakdown procedure, as was previously explained.

Also, in this study we wanted the computer generated materials to better represent structures obtained experimentally (and for which we are now obtaining experimental values). Thus, it was necessary to modify our codes to allow the generation and simulation of materials containing fibers of much higher aspect ratio but in lower concentration than we had used before.

The parameters used to create these materials are shown in Table 3.

Table 3 – Material parameters for the study of the breakdown path formation

Concentration	7.8E-6, 2.3E-5
Volume	216 μm^3
Fiber length	1 μm
Radius	14,0 nm
Voltage drop	0.01 Volts

In the simulations we observed that the breakdown paths follow a minimum distance pattern, and only deviate from this law when the permittivity is very high and the dielectric breakdown occurs for the initial voltage.

This assumption can be verified by using the maximum common sub-graph (mcs) metric. To use that metric, we build a graph extracted from minimum distance paths in the original graph. For that, we employ a modify version of the APAC algorithm and apply it to the initial graph in order to extract the same number of minimum distance paths than the breakdown paths. Then we apply the mcs metric and it provides us with the degree of isomorphism between the two graphs. If the graph built from the breakdown path is isomorphic to the graph built (with same number of paths) from the minimum distance paths, then the breakdown procedure follows a minimum distance pattern and the returned value of this metric should be zero. A larger return value indicates that the breakdown deviates from a minimum distance pattern.

Another result than can be extracted from the previous simulations is that the breakdown starts on one plate and propagates to the other plate, as is shown in Figure 22. This can be seen by the number of nodes connected to the source and sink nodes (enter and exit nodes). It is also important to note that the permittivity increases with progressing dielectric breakdown, as we can see in Table 4 from the value of the permittivity immediately before the last breakdown step occurs.

Table 4 – Permittivity values for selected time steps. Each step corresponds to an interval in the voltage.

Time Step	Permittivity
Step 1 = [0.01,0.31[Volts	8.2338
Step 2 = [0.31,12.94[Volts	12.5183
Step 3 = 12.94 Volts	∞ (breakdown)

| Time step 1 | Time step 2 | Time step 3 |
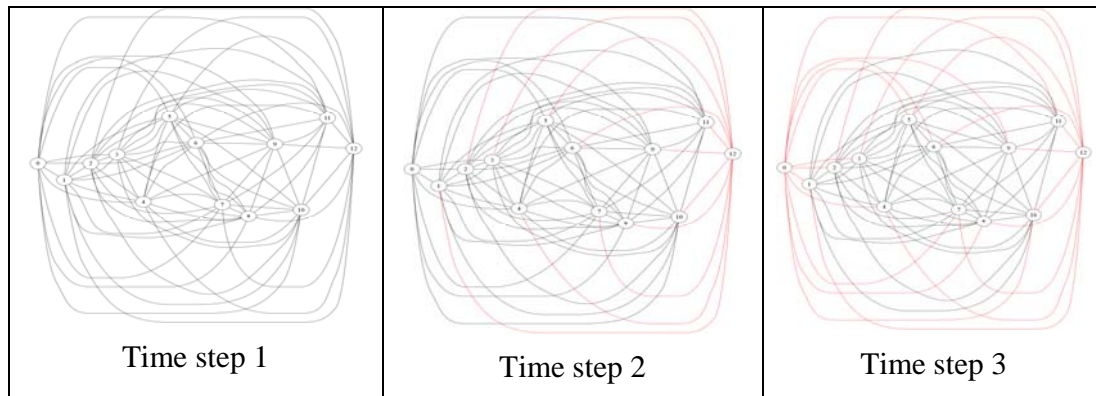
Figure 22 – Graphs of the nanofiber network system at different time steps along the simulation.

Additional considerations in the framework of this study:

- The simulations also indicate that the capacitor plate model is not a good procedure for trying to experimentally measure the permittivity, due to dielectric breakdown phenomena. Fibers near the plates tend to suffer breakdown, resulting in over-estimation of the permittivity for that specific concentration in high aspect ratio fiber networks.

- In the analysis of the breakdown mechanism in nanocomposites with high aspect ratio fibers, the performed simulations demonstrate that the dielectric breakdown process stalls after some number of iterations. When this happens, the permittivity is at high values and remains so until a conductive path is formed, terminating the avalanche process. In theory, this phenomenon could be used to increase the permittivity of a nanocomposite like the ones modeled, without decreasing the dielectric strength (and using lower concentrations than typically used for these materials). For this, one would have to cause

partial dielectric breakdown in a high aspect ratio and low concentration nanocomposite, that is, to cause local dielectric breakdown to start occurring and then stopping the dielectric breakdown process when there is no change in permittivity. This should lead to high permittivity and relatively high dielectric strength composites at low concentrations.

- With this concept in mind, it should also be possible to design a sensor that with a constant applied voltage can retrieve a signal whenever tension is applied to the plates. Again this would require stopping the dielectric breakdown process before it creates a complete conductive path. At that point, the dielectric gap between one of the plates and the last fibers along the incomplete conductive path will be small with higher polarization, and any small (compressive) displacement of the plate will enable a contact and thus the final breakdowns process. The main difficulty will be to control experimentally the optimal distance at which this process occurs.

- All these considerations will be further investigated during the next semester.

Integration test and the relation with algorithm speed

During the previous months we have exhaustively tested the numerical error of the integration code, and we found the code to be very sensitive to two numeric errors. Thus, a study to test the best integration scheme was needed. Figure 23 shows the error tests for the integration of:

$$\iint_{\Gamma} \frac{1}{\left\| \vec{r}' - \vec{R} \right\|} dS'$$

In Figure 23 we can see how the error of the Gaussian quadrature (with different quadrature degrees) behaves when $\left\| \vec{r} - \vec{R} \right\| \to 0$. The description of the quadratures used in Figure 23 are described in Table 5.

Table 5 – Used quadrature rules.

Quadrature rule	Degree	Integration points number
Q2	2	3
Q4	4	6
Q6	6	12
Q8	8	16
Q10	10	25
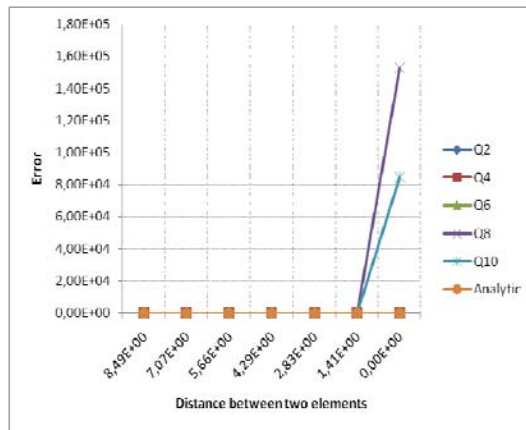
Figure 23 – Effect of the distance between elements on the integration error.

We also see that an analytic version of the integral [14,15] has a bound error, but it is quiet mathematically expensive to calculate. In our approach, we use the Gaussian quadrature of degree four with six integration points when $\left\|\vec{r}'_{barycenter} - \vec{R}\right\| > 2.0\,nm$, and we use the analytic version when it is lower.

Shortest path problem and comparison with the Yen algorithm
For implementing a procedure to answer the question of whether the dielectric breakdown path follows a minimum distance pattern, it was necessary to implement a minimum path distance algorithm. The state of the art refers to the Yen [16] algorithm but that implementation cannot be used in directed and undirected graphs. With this limitation in view, we have decided to develop a version of the APAC that can be used for the two types of graphs. We report the comparison of the developed algorithm with Yen's in Figure 24.
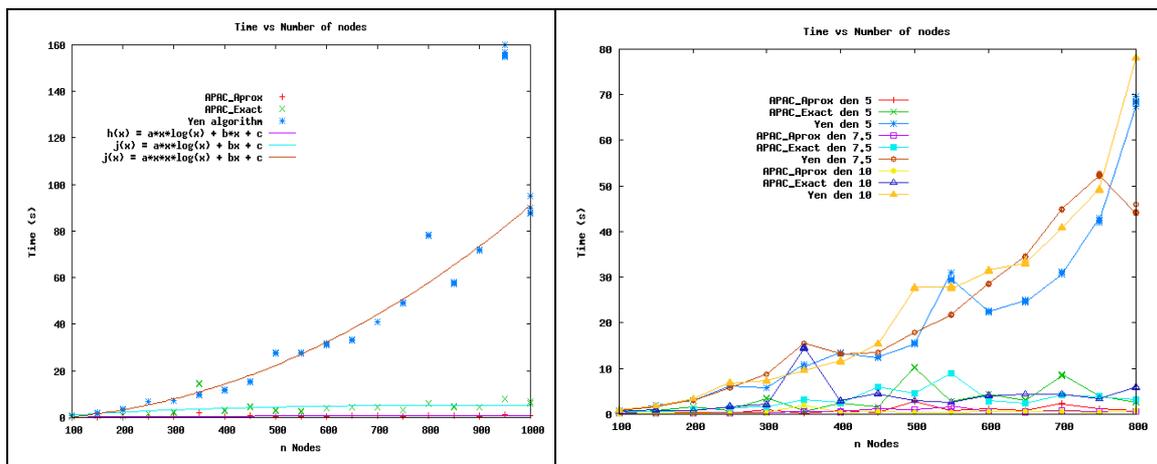
Figure 24 – Comparison of algorithm performance between our approach (APAC) and Yen's.

Figure 24 shows that our algorithm is faster when the graphs are small. However, for large graphs (with a large number of edges) our algorithm suffers relative reduction in performance. We know how we could increase the performance for these cases, but as the current implementation fits our needs it has not been implemented so far and is not scheduled to be implemented in the near future. The reported algorithm has a high degree of application (minimum path distance) to other areas like transport network, network routing and others.

Numerical method validation: study of the effect of fiber concentration on the permittivity and dielectric strength

In this section we demonstrate the validation of the developed numerical methods. The simulation was compared to in-house (department of physics) experimental results and also to experimental results from the literature.

As any model it is necessary to validate it, by comparing with analytic expressions and/or experimental results. The developed model can be broken in two parts, one related with capacitance extraction problem and the solution of the network problem. The validation procedure is described in this section by comparing the numerical results for several existent analytic solutions and experimental results.

The analytic solution for sphere self capacitance is well known and can be found using Gauss law and with the capacitance definition. For sphere with radius r located at the origin, a Gaussian spherical surface with radius R is constructed. For R = r by using the Gauss law the electric field is given by: $\vec{E} = \dfrac{Q}{4\pi\varepsilon_0 r^2}\hat{r}$ where Q is the total charge.

Integrating along a radial direction: $\Delta V = \dfrac{Q}{4\pi\varepsilon_0}\int \dfrac{1}{r^2} dr = \dfrac{Q}{4\pi\varepsilon_0 r} + const$. The constant is related with the some reference potential, considering that reference potential is at the infinite then const = 0. Typical the later integration gives two 1/r terms if one this terms is at the infinite it is fair to consider 1/r → 0. Using the capacitance definition $C = \dfrac{Q}{\Delta V}$ yields the analytic expression for the sphere self capacitance $C = 4\pi\varepsilon_0 r$. The numerical result for the sphere self capacitance meshed (2048 triangles) with radius equal to 1.0 m yields 0.111607 nF. The analytic solution using the same radius as input in Eq 5.4 is 0.112086 nF. The relative error is then ~0.4 %.

The capacitance for a parallel plate in vacuum is given by, $C = \varepsilon_0 \dfrac{A}{d}$. For plates where the area (A) is equal to 1 m^2 and the separation between then is 0.1 m, the capacitance is 8.854E-2 nF. The numerical results using a mesh with 1024 triangles yield 8.193E-2 nF. The relative error is then ~7%. Comparing the error with a single sphere (0.4 %) and two

spheres (0.7%), describe later, it can be seen that the value is higher; this is expected by analyzing the charge distribution in Figure 34 (right). In Figure 34 (right) the corners of the plates demonstrate the expected accumulation of charge, to reduce the error it is necessary a finer mesh or more triangles near the corners and edges.

There is no analytic solution for the capacitance between to spheres, but a good approximation for the problem is given in [1]. The author uses a successive application of the image charge method. The truncated series is then: $C = 4\pi\varepsilon_0 \dfrac{a^2}{d}\left(1 + \dfrac{a^2}{d^2 - 2a^2} + \dfrac{a^4}{d^4 - 4d^2a^2 + 3a^4}\right)$. The parameters for this Equation are presented in Figure 25. For two parallel spheres with radius (a) equal to 1.0 m and center-center separation distance (d) equal to 3.0 m using the later equation, gives a capacitance of 0.1271316 nF. The later value for the total capacitance is the sum of the mutual capacitance plus the capacitance at the infinity or the self capacitance of the sphere. For a parallel spheres with r = 1 m and center-center separation equal to 3.0 m the numerical results as the 0.1280129 nF. The relative error is then ~0.7 %.
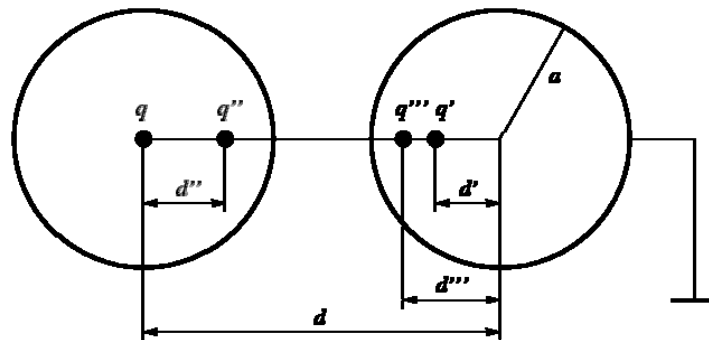
Figure 25 - Geometry used for the calculation.

In Figure 26 (left) are shown the experimental and simulation results of the dielectric constant for several concentrations. The simulated dielectric constant has a scaling difference of 1E6 relative to the experimental values. This is expected, as in the proposed algorithm only cylinder-cylinder capacitances are calculated, and it is assumed that inside the cylinder the dielectric constant is the same as the lossless matrix. These simulations were made using cylinders with an aspect ratio of 10 (14 nm and 140 nm for the length).

[1] Wasshuber, C., *About Single-Electron Devices and Circuits*. 1997, Wien: Technischen Universität Wien.
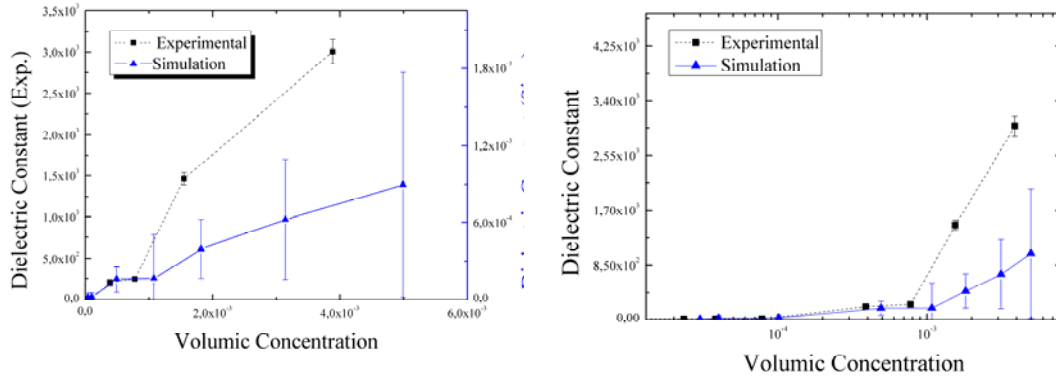
Figure 26 - Experimental and simulated dielectric constant versus filler volume concentration (left). Experimental and normalized simulated dielectric constant (right).

Due to these approximations, Figure 26 also shows (on the right) the normalized simulation results using the following equation.

$$\varepsilon_n = \varepsilon_{PVDF}\left(\frac{\varepsilon - \varepsilon_{\min}}{\varepsilon_{\min}} + 1\right)$$

The trends and values of the simulation are similar to the experimental ones. The experimental values refer to MWCNT/PVDF composites with an average aspect ratio of 10. This aspect ratio was obtained during the fabrication process. We use these experimental values to validate the numerical procedure. It can be observed that the critical concentrations are similar; in the simulation it is 0.0011 and in the experiments 0.0016 (2.0 wt%). These concentrations disagree with the multi wall carbon nanotube/poly(vinylidene fluoride) - MWCNT/PVDF - composite study by Wang and Dang [17] (0.0161), and are more in agreement for the same type of composites with Ahmad [18] (0.0079).

Using the following equation $\varepsilon_{eff} = \varepsilon_0(f_c - f)^{-s}$, valid for $f \leq f_c$, we found that the best fit using a non linear least square algorithm in a log-log plot of the dielectric constant, which yields *s = 0.29 +/- 0.09* for the simulation and *s = 0.22 +/- 0.09* for the experimental values without normalization. Using the critical concentration from the experiments, the simulation results yield *s = 0.28 +/- 0.09*. These exponents and the corresponding errors are in the same interval, validating the assumption that highly dispersed MWCNT nanocomposites form capacitor networks. Comparing with MWCNT/PDVF exponents *s = 0.31* [17] our data error interval includes the later value, but disagrees with the universal value for the superconductivity exponent (0.75).

The fitting error is large, indicating that the power law $\varepsilon_{eff} = \varepsilon_0(f_c - f)^{-s}$ is not accurate enough to predict the composite dielectric constant. The dielectric constant is expected to

increase with filler content when approaching the percolation threshold for small concentrations and decrease above the percolation threshold. The later is in disagreement with our experimental and simulation results and with the percolation law. This type of behaviour has also been observed for composites of polycarbonate and either MWCNT or carbon black; as reported in [19] and references there in. They also found a low percolation concentration between 1.0 – 1.5 Wt%. For the same type of composite (MWCNT/PC) a low percolation value (1.0 – 1.5 Wt%) was also reported in [20].

The previous sections show that for low variations in the minimum tube-tube distance, below 45 nm in the initial separation, the capacitance has a higher increase for the same variations at distances larger than 45 nm. Thus, the critical concentration is related to the MWCNT orientation and minimum tube-tube distance. It should also be noted that, in the present simulation, contact between the fillers was not allowed. In this case, it is clear that the increase in the permittivity and the critical concentration is not related with the formation of "contact" networks, but simply with geometrical factors related to the capacitance. After the critical concentration, the simulation diverges relatively to the experimental values. In this regime, the probability of contact between MWCNT is very small or not possible [21] but we cannot state the same for the contact between MWCNT clusters. Similarly, in real situations, it is not possible to have a single aspect ratio in the MWCNT but a distribution of aspect ratios.

Another important topic is the deviation bars found in Figure 26; these are related with the effect of the minimum distance and rotation angle previously explained. For higher concentrations the deviation increases. As the separation between MWCNT decreases, small changes in the distance result in a strong change in tube-tube capacitance.

The high value of the critical concentration in [17] relatively to the ones found in the present work is high enough to indicate the formation of a "contact" network [21]. This fact may explain the superb agreement between the experimental results of [17] and the percolation law. Also, based both on our results and on [19], it can be stated that for low values of the critical concentration, the percolation law is not accurate in describing the dielectric constant of the nanocomposite.

Figure 27 (right) shows that the external voltage required to enable the formation of a conductive path decreases with the filler volume fraction. The error bars associated with the voltage calculation are also displayed and show significant variations for small concentrations. This can be explained by noting that the orientation of each conductor influences the local capacitance of the composite; also, in the materials that were generated, small variations in the filler-filler minimum distances induces the relatively large changes in breakdown. These two factors contribute to the large deviations of the overall values
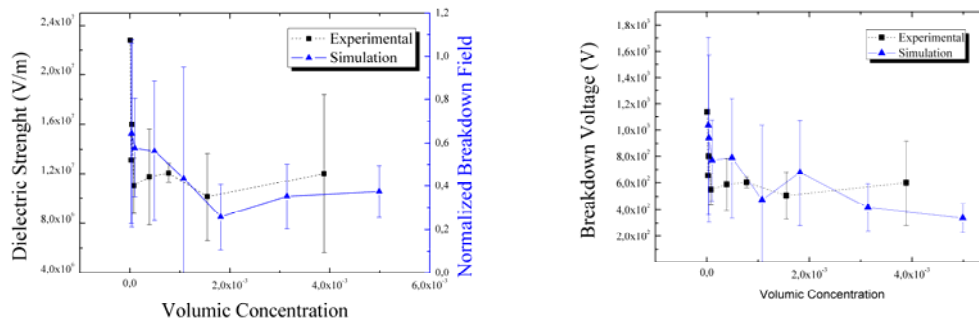
Figure 27 – Experimental dielectric strength and normalized breakdown field versus filler volume concentration (left). Simulated breakdown voltage versus filler volume concentration (right).

Figure 27 (left) shows the normalized breakdown field using the experimental dielectric strength of the polymer, in the range of 2E8 V/m. The plot shows that the breakdown field decreases with the concentration. Thus, the external breakdown voltage that is required for the formation of a conductive path decreases with the filler volume concentration. These results are in agreement with trends presented for spheres in [10 - 11], through modelling and experimental testing. The last concentration in the numerical results cannot be obtained experimentally, as for these concentrations the nanocomposite is already conductive.

Figure 28 shows that the average minimum distance is a good parameter to estimate the optimal separation that enables a high dielectric constant and a high breakdown field. Using this parameter we can now start to connect some experimental measurements to the average minimum distance.
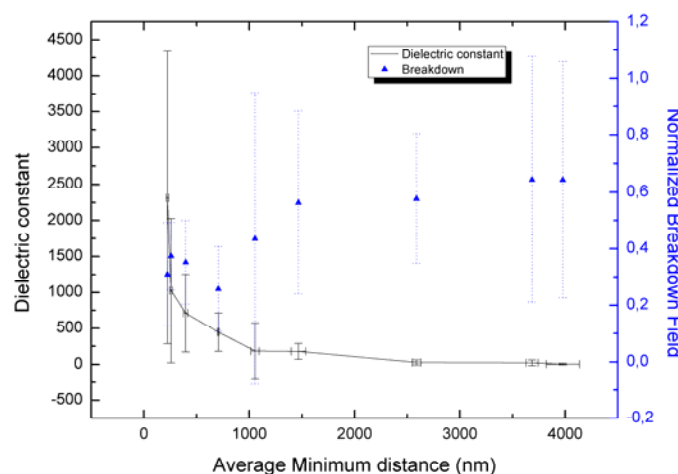

Figure 28 – Variation of the dielectric constant and the normalized breakdown field with the average minimum distance

Study of the nanocomposite network electric anisotropy

In this section we explore further the model by generating nematic material with an aspect ratio of 10. To generate a nematic state material we restrict the z component to a value larger than 90% of the cylinder length. Figure 29 represents this type of the material (aspect ratio 10).
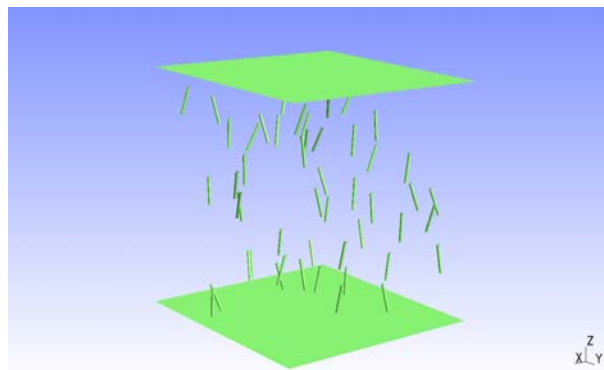
Figure 29 - Representation of a nematic state material

For the nematic state we can see (Figure 30) that the value of the dielectric constant is lower than random generated materials and in the same figure the standard deviation is also small compared with random ones. This can be explained by alignment of the cylinder in the nematic state which restricts the role of rotation in the overall capacitance, as had been discussed later. The capacitance is higher for a pair of perpendicular cylinder, so by restricting the orientation we are lowering the capacitance and thus lowering the overall permittivity. The random materials exhibit high standard deviation, as the spatial arrangement of each specific cylinder network affects its properties in a significantly way. This behavior for the nematic state material will be studies in the following section for an aspect ratio of 50 with a higher number of concentrations.
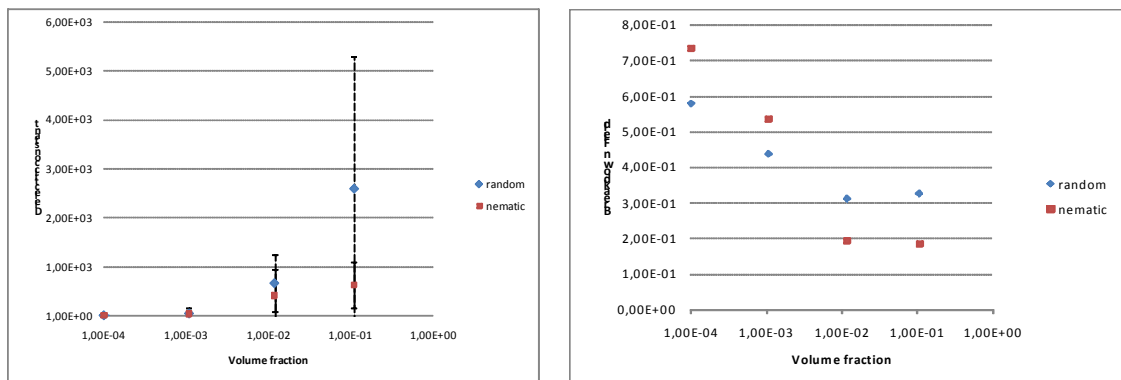
Figure 30 – Dielectric constant (left) and normalized breakdown field (right).

Figure 30 shows an inversion in the breakdown field at the concentration of 0.01. Comparing to the values in Figure 30 (left) for the same concentrations, and since the dielectric constant did not change, this must be related to orientation of the fibers in the nematic state near the plates of the capacitor. We can see in Figure 16 that for $\pi/2$ the capacitance is higher than other orientations, this enables stronger fields in this region, which triggers the cascade procedure for lower applied voltages than in the case of the random materials.

The influence on aspect ratio in the composite the electric properties has been addressed in recent experimental article by Sheng-Hong et al [22]. The authors studied electric properties of poly(vinylidene fluoride) (PVDF)/MWCNT composites, namely the influence of the aspect ratio in the dielectric constant. They found that increasing the aspect ratio increases the dielectric constant and the percolation threshold, and also that the percolation threshold deviates from the predictions from the exclude volume theory (Figure 31). The authors explain these deviations with the formation of clusters, which will give higher critical concentrations.

A recent review in carbon fiber composites also addresses the problem of the multiple values for the critical concentrations in the same type of composites [23].
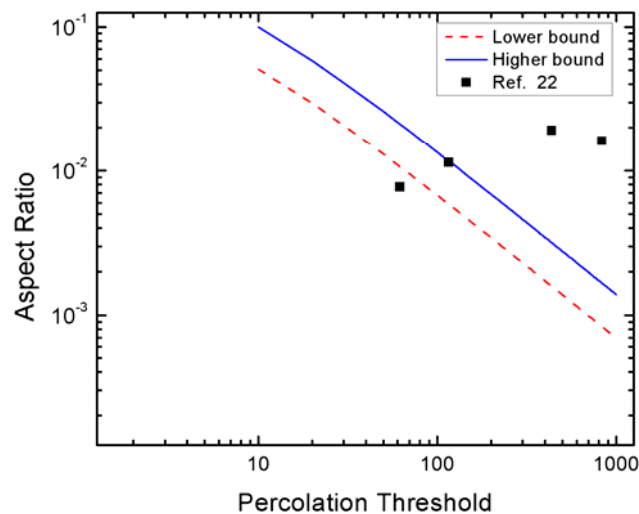
Figure 31 - Comparison of the bounds of the exclude volume with the Ref 22.

In this section we study the influence of the aspect ratio and the orientation in the dielectric constant. For that we generate isotropic and nematic materials. As described in the previous sections we start by generating the microstructure by randomly placing cylinders with an aspect ratio of 50 (14 nm diameter and 700 nm length) for the isotropic materials. For the nematic state materials we constrain the zenith angle between 0º and 20º degrees and randomly place the cylinders in domain. A minimum separation threshold of 1.0 nm was also defined with the purpose of not taking into account quantum

tunneling effects. The value for this threshold is based on predictions of the order of the tunneling distance as 10 Å [24]. For each concentration we average ten different materials. We also use a large value for the average degree. Finally, the matrix dielectric constant was set to 7 (based on ε_{PVDF}).

In Figure 32 we present the results for the dielectric constant of random and nematic materials. Observing the error bars we can conclude that the statistical error is higher for the random materials. This is related to the effect of the minimum distance and the rotation angle in the local capacitance as previous explained in section 4 ("Effect of the fiber orientation and average distance on the capacitance"); for the anisotropic materials we observe a reduction in the statistical error due to the orientation of the cylinders. Also based in the same figure we can conclude that: a) increasing the average degree will increase the dielectric constant; b) the nematic materials have a lower dielectric constant comparing with the isotropic ones; this can also be observed in [25] for the conductivity.
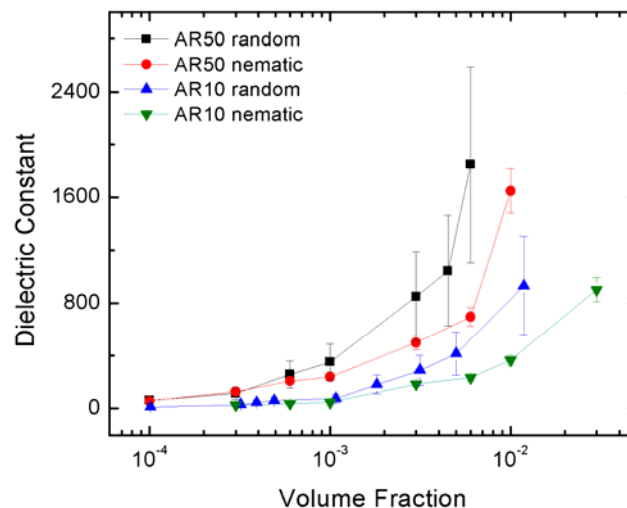
Figure 32 - Comparison of random and nematic materials with an aspect ratio of 50 and 10.

In Figure 32 one can observe that the nematic materials exhibit lower dielectric constant than the isotropic ones.

The fact that nematic materials show a lower dielectric constant than the isotropic ones (Figure 16) is related to the zenith angle. In section 4 ("Effect of the fiber orientation and average distance on the capacitance"), we demonstrate that parallel cylinders exhibit a lower capacitance, so the lower value for the composite dielectric constant is related to the filler alignment.

It should be noted that by using a high average degree our graphs are almost complete removing the effect of different network topology in the results, *i.e.*, the number of serial or parallel capacitors in the network is roughly the same for each material.

Using the results in Figure 32 we can fit a power law to the two nematic materials (AR 10 and 50). For the nematic AR 50 materials the linear fit in a log – log plot has a slope value of 0.67 ± 0.48 and an intercept value of 4.43 ± 0.16. For the nematic AR 10 materials the slope is 0.61 ± 0.48 and the intercept 3.77 ± 0.56. The adjusted R-square for nematic AR 50 and AR 10 were 0.97 and 0.99. The later values indicate that the dielectric constant follows a power law, $y(x) = ax^b$; in Figure 33 (inset) we show the log-log plot for the two types of nematic materials. The b exponent should have a lower error in order to achieve meaning in terms of physical features. Still, the values are similar for both materials. A larger number of simulations would help decrease the exponent.

As was previous found by Hu *et al* [26], for the conductivity, the a constant is related with aspect ratio. It can be seen that the a constant for the AR 10 is 4.56 (~5) times greater than the AR 50 one, so the a constant is related with filler aspect ratio supporting the results of Hu *et al* [26]. Also by dividing the a constant with a suitable factor we can empirically find lower or high aspect ratios using the mentioned power laws.

We can further test the later assumptions by comparing with related experimental work for MWCNT/PVDF composites. In Figure 33 we divided the nematic AR 10 power law by 2 and 4; this gives an aspect ratio of 5 and 2 as previous discussed. Using the AR 50 power law yields similar results. The results in Figure 33 demonstrate that the formation of clusters in conjugation with fiber breaking due to the fabrication process will reduce the fillers effective aspect ratio by several orders of magnitude. Also, an increase in the filler aspect ratio is observed with the MWCNT volume fraction. The decrease after the critical concentration observed in Figure 33 for an aspect ratio of 833, could be related with a reduction in ratio filler length/domain length as can be observed in a recent work [27]. This will be further explored in the following section.
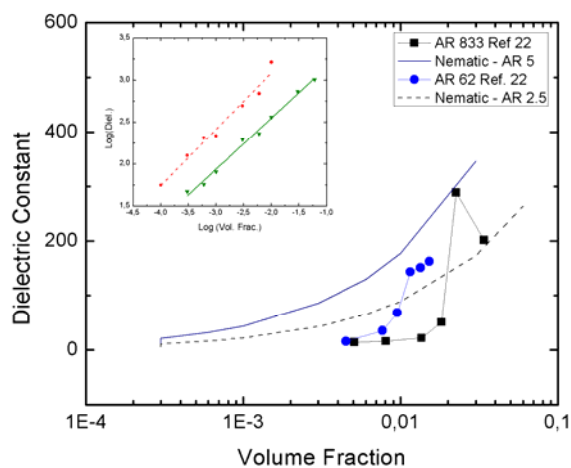

Figure 33 - Comparison with experimental work and the empirical law.

In summary, we found that the formation of clusters and the MWCNT breaking due to the fabrication process can reduce the fillers effective aspect ratio. We also demonstrate that the continuous increase of the dielectric constant is related with the formation of a capacitive network where the long range Columbic interactions prevail and the reduction in the composite dielectric constant after the percolation threshold could be related to a decrease in filler length/domain length ratio.

CAD integration

New visualization capabilities were also developed for the representation of the conductors charge distribution. In these new routines a new interface with some CAD mesh output formats was also developed, enabling the representation of complex geometries.
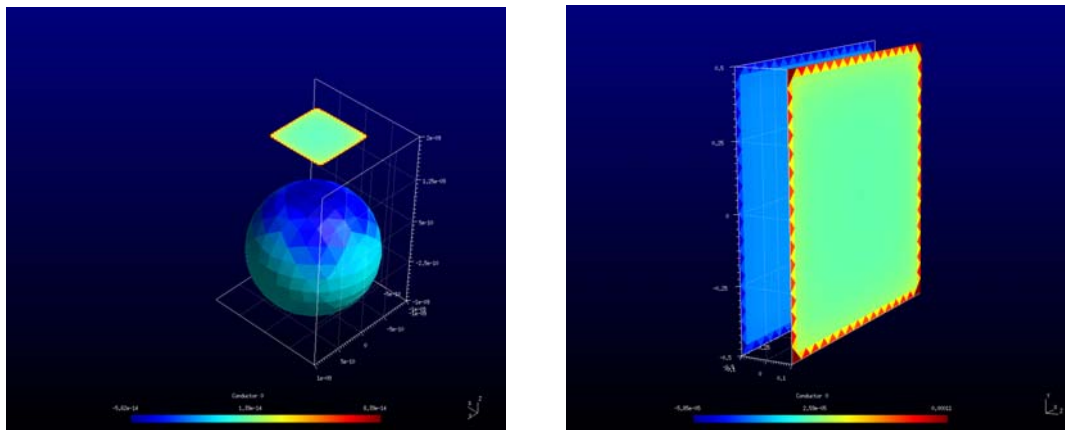
Figure 34 –The represented figures display the charge distribution when one conductor is raised to 1 volt and the other grounded. Note the edge effects on the plate; these can be used to validate the developed numerical routines.

Study of the role of the percolation law in carbon nanofibers, MWCNT composites. Understanding the mechanisms behind percolation without contact.

In order to better understanding the proposed mechanism, let us briefly review some essential concepts.

The percolation theory goes back to World War II with the studies of polymerization process by Flory and Stockmayer. They studied the gelation process that occurs when polymerization leads to the formation of a network of chemical bounds spanning the domain. The name and the formal concepts where introduced by Broadbent and Hammersley.

The fundamental concepts in the percolation theory are the percolation threshold (p_c) and the existence of correlation length that rules critical phenomena. The percolation threshold is defined as the concentration p at which an infinite cluster appears in an infinite lattice. For a concentration $p > p_c$ a cluster spans the system, whereas for $p < p_c$ the spanning cluster does not exist and the system is made of many small clusters. The models usually employed to study the spanning cluster are the "site percolation model", where each site is randomly occupied with certain probability, and the "bond percolation model", where for a given probability each line in the lattice has an open or a close bond. In both cases, the statistical properties of the clusters and the infinite cluster are studied. The relation with neighbor sites and the average cluster size (S) are also relevant for the percolation theory. The average cluster increases with concentration as we approach the percolation threshold and at the percolation threshold diverges ($S = \frac{1+p}{1-p}$, $p < p_c$). We can also relate the average size with a correlation function. The correlation function, $g(r)$ is the probability that a site at a distance r from an occupied site is also occupied and belongs to the same cluster. The second moment of the cluster size distribution equals the sum some over the correlation function [28]. Thus we can define the correlation length (ξ) as the cluster radius that gives the main contribution to the second moment of the cluster size distribution near the percolation threshold:

$$\xi \propto |p - p_c|^{-v}$$

The exponent v has the value ~0.88 for 3D percolation; the latter is described in more formal and extended way in [28].

As the concentration increases, the correlation length increases and, at the percolation threshold, diverges. For $p > p_c$ a cluster appears that is infinite in extent. The numerical value of p_c depends on the dimensionality of the lattice and on the lattice type. The critical exponent v depends only on the domain dimension. It can be seen in the derivation of the later equation that the correlation length is intrinsically connected with the cluster size, and the cluster size can be easily related with the cluster radius. The correlation length can also be seen as the radius of those clusters that have a stronger contribute to the divergence or the radius of gyration of the largest cluster. For $p > p_c$ the correlation length is related to the radius of the largest hole in an infinite cluster. The existence of only one length that dominates the critical behavior is the foundation of the percolation theory.

As stated before, the percolation threshold depends strongly on the geometric nature of the domain in study. It is also believed the critical exponents are universal, for some dimension – a triangular lattice and square lattice will have the same numerical value for the critical exponents. At the percolation threshold there are several physical properties that can diverge, for instance the conductivity and the dielectric constant. The relation to the composite critical concentration in the conductivity and the dielectric constant was earlier studied by Bergman and Imry in 1977 for heterogeneous mixtures of a conducting phase and an insulating matrix. An important result in this work is the divergence at the percolation threshold. The critical exponents γ, β characterize the percolation phase transition at $p = p_c$. The exponent β characterizes the abrupt peak on the correlation length. The exponent γ characterizes how the average cluster size diverges. The constant B are coefficients of the scaling functions F_+ and F_- that can be experimentally determined by measuring the composite effective dielectric constant. Bergman and Imry

also explained that the physical meaning of the effective dielectric constant divergence is related to the existence of conductive channels stretching across the entire length of the system. This theoretical prediction was later completed in a following work by Bergman and Stroud [29], which using a scaling assumption analyze the critical behavior of the composite dielectric constant. The scaling assumption is valid for $|\varepsilon_1/\varepsilon_2| << 1$ and $|p - p_c| << 1$. Bergman and Stroud demonstrate for metallic inclusions in an insulating matrix the dielectric constant as a peak at ω = 0 Hz, the height of which is proportional to $\varepsilon_{matrix}|p - p_c|^{-s}$, diverging at p_c. The later yields a well known relation that holds for p < p_c and p > p_c $\varepsilon_{eff} \propto \varepsilon_{matrix}|p - p_c|^{-s}$ .In the same article [29] Bergman also demonstrates, using the same scaling relations, that for p > p_c the composite conductivity is given by the following relation: $\sigma_{eff} \propto \sigma_{matrix}(p - p_c)^t$

On later equations *t* and *s* are called the conductivity, t, and superconductivity, s, critical exponents. The values for the conductivity exponent (t) were determined by Kirkpatrick [30] using three different models. The value for 3D system was 1.5 +/- 0.2 in more recent works the accepted value is ~1.8. For the superconductivity exponent using a bond percolation model, in 3D system, in conjugation with a transfer matrix algorithm, Herrmann and Derrida [31] found that the value is 0.75 +/- 0.04.

In relation to the percolation theory, there are new insights regarding the universal nature of the critical exponents. In a recent paper, Myroshnychenk and Brosseau [32] used a Monte Carlo method coupled with a finite element method, demonstrating non universal values in 2D for the conductor and the superconductor exponents. They showed, for 2D discs with varying degree of penetration, the *s* exponent could be higher than *t*, breaking the universal nature of the exponents, i.e., in 2D s = t. Later, when reviewing some experimental results, the work presented here shows that critical exponents deviate from the universals values predicted by the percolation theory.

For high aspect radius fibers Berhan and Sastry [33,34] studied the connection between the percolation threshold and excluded volume theory using Monte Carlo simulations. They demonstrate that the hard-core modeling approach is more appropriate for modeling composite materials in which the main charge transport mechanism is tunneling. They also found strong dependence on the tunneling distance for the percolation threshold.

Finally, there are some open questions in relation to the existence of an infinite cluster (at the percolation threshold) in 3D [35] and the behavior of the critical exponents [36].

To study the mechanism we used the experimental results of [37]. The authors studied MWCNT in a PVDF. The interesting point in this work is that the nanotubes were functionalized which will improve the adhesion to the matrix and possibly the filler dispersion.

For this study we generate 50 random materials for each concentration, with an aspect ratio of 10. *A posteriori* we select the best materials that approximate the experimental ones. We analyze the microstructure and conclude that a change in the anisotropy in conjunction with a decrease of the ratio filler length/domain length leads to the increase and later decrease of the dielectric constant.

In Figure 35 we fit a Gaussian to the numerical and experimental results. The adjusted R-square has the value of 0.94 and 0.97 for numerical and experimental results. The sigma has the value of 0.02, the full width half maximum has the value of 0.05 and the value for x_c is 0.14 for both results.

In order to confirm the latter assumptions a new set of simulations are being carried out, focusing in the anisotropy in each concentration, where the Herman's orientation function $\langle P_2(\cos\theta)\rangle$ is used to characterize each material.

$$\langle P_l(\cos\theta)\rangle = \frac{\int\limits_0^{\pi/2} P_l(\cos\theta)N(\theta)\sin\theta d\theta}{\int\limits_0^{\pi/2} N(\theta)\sin\theta d\theta}$$

Where P_l is the Legendre polynomials in $\cos\theta$, and $N(\theta)$ is the orientation distribution function.
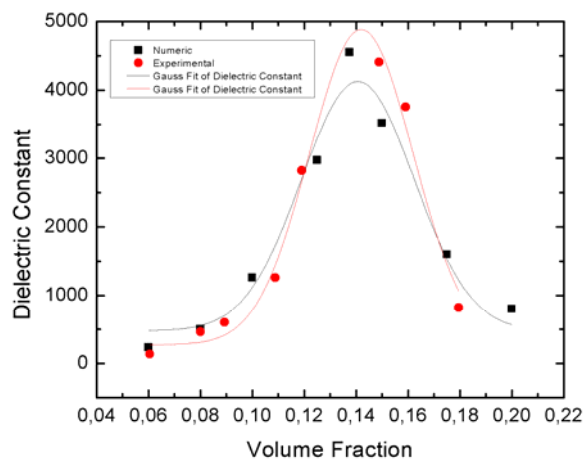

Figure 35 – Fit of a Gaussian to the experimental and numerical results.

5. Conclusions

The Graph Theory presents interesting applications to the study of the electrical properties of nanofiber-reinforced polymer matrices.

We can identify and characterize probable conduction paths in a nanofiber network, and study the effect of microstructural features on the properties.

The nanofiber network arrangement and material parameters (concentration, length and orientation of the nanofibers) affects the conduction paths and, thus, affects the electrical behavior of the material.

A larger number of simulations is required to establish conclusive trends, and further work is required to obtain macroscopic properties comparable to experimental results.

The results so far seem to indicate that for high aspect ratio fibers, by interrupting the dielectric breakdown mechanism when there is no change in the permittivity, it might be possible to obtain materials with high permittivity and relatively high dielectric strength at low concentration values.

It was shown that below the critical concentration, highly dispersed conductive fillers form capacitor networks.

It was demonstrated that the dielectric constant and the dielectric strength of the composite are highly dependent on the distribution of the fillers, resulting in high deviations of the electrical properties.

It was concluded that the percolation law is not always the most accurate description at the critical concentrations for this type of nanocomposites. Namely, from the percolation law, the dielectric constant is expected to increase with filler content when approaching the percolation threshold for small concentrations and to decrease above the percolation threshold. This type of behaviour is an open question for this type of composites [19].

It was found that the increase and the decrease of the dielectric constant after the percolation threshold can be related to a variation in the anisotropic state of the composite due to the increase of the filler concentration. Also, that decrease of the dielectric constant after the percolation threshold can be related to an increase in the effective aspect ratio of the fillers. This new possibility follows a Gaussian law and can be tested with the developed numerical procedure.

6. Ongoing and envisioned tasks

Although the project was completed in March 2009, the work has spawned some new questions that would be interesting to pursue. Thus, we consider as possible further tasks, which can be developed in the scope of a subsequent project:

- Study of the topology of the breakdown for larger volumes.
- Generation of larger set of materials and orientations for each concentration, to increase the confidence in the simulation results and improve the accuracy of some curve fitting.
- Effect of mechanical strain on the electrical and dielectric properties.

7. Scientific output

Below we list the scientific output that resulted from this project.

Papers in Scientific Journals

- Simoes, R.; Silva, J.; Vaia, R.; Sencadas, S.; Costa, P.; Gomes, J.; Lanceros-Méndez. S.; Low percolation transitions in carbon nanotube networks dispersed in a polymer matrix: dielectric properties simulations and experiments, Nanotechnology 20 (2009) 035703.

- Simoes, R; Silva, J.; Cadilhe, A.; Vaia, R.; Applications of the graph theory to the prediction of electrical and dielectric properties of nano-filled polymers, Composite Interfaces 2009, accepted

- Simoes, R.; Silva, J.; Vaia, R.; A complex network based simulation approach to predict the electrical properties of nanocomposites. Journal of Nanoscience and Nanotechnology 2009, accepted

Papers in International Conference Proceedings

- Simoes, R.; Silva, J.; Cadilhe, A.; Vaia, R.; A Computational Method to Explore the Breakdown Process of Conductive Fillers in a Lossless Dielectric Nanocomposite; in Proc. ICCMSE 2008 - International Conference of Computational Methods in Sciences and Engineering, Hersonissos – Greece: 25-30 September 2008

- Simoes, R; Silva, J; Cadilhe, A; Vaia, R; Applications of the Graph Theory to the Prediction of Electrical and Dielectric Properties of Nano-Filled Polymers; in Proc. Eurofillers 2007 – Functional Fillers for Advanced Applications , Zalakaros – Hungary, 26-30 August 2007

- Simoes, R.; Silva, J.; Dias, G.R.; Vaia, R.; Effect of the Nanofiber Network Arrangement on the Properties of Polymer-Based Nanocomposites; Proc. IV International Materials Symposium, Aveiro, Portugal, 2-4 April 2007

Papers in Preparation

- Scripta Materialia (scheduled for submission in April 2009)
- Physical Review B (scheduled for submission in June 2009)
- Physical Review Letters (scheduled for submission in August 2009)

Invited Presentations at International Conferences

- Cunha, A.M., Simoes, R., Silva, J; Nanofiber-reinforced polymeric systems: prediction of the properties strain dependence; POLYCHAR 15 - World Forum on Advanced Materials, Buzios, Brazil, April 2007

Oral Presentations at International Conferences

- Eurofillers 2009, Alessandria, Italy, June 2009 (accepted)
- Materials 2009, Porto, Portugal, April 2009 (accepted)
- ICCMSE 2008, Hersonissos, Greece, September 2008
- Eurofillers 2007, Zalakaros, Hungary, August 2007
- Materiais 2007, IV International Materials Symp., Porto, Portugal, April 2007

Poster Presentations at International Conferences

- Nanospain 2009, Zaragoza, Spain, March 2009

Other Presentations at Scientific Events

- June 1, 2007 – Dielectric Polymer Nanocomposite Workshop, Wright Brothers Institute – Innovation and Collaboration Center, Dayton, Ohio, USA, entitled "Graph theory applications for the prediction of electrical and dielectric properties of nano-filled polymers".

Theses

- March 2009, Electric and dielectric properties of carbon fiber networks dispersed in a polymer matrix, Jaime Silva, Masters' Thesis, University of Minho, Portugal

8. Disclosure of inventions

We certify that there were no subject inventions to declare during the performance of this grant.

References

1. Mark F. Gyure and Paul D. Beale. Dielectric breakdown of random array of conducting cylinders. *Physical Review B*, **40**:9533–9540, 1989.

2. Witold Brostow, Antonio M Cunha and Ricardo Simoes. Mater. Res. Innov, 7:19, 2003.

3. Philipse AP. The Random Contact Equation and its implication for rods in packings, suspensions, and anisotropic powders. Langmiur, 12:1127-133, 1996.

4. Tsu-Wei Chou, Erik T. Thostenson and Chunyu Li. Composites Science and Technology, 65, 2005.

5. András Recski. Matroid Theory and its Applications. Springer-Verlag, 1989

6. L. Greengard, H. Cheng and V. Rokhlin. Journal of Computational Physics, 155 468 1999.

7. Songmin Kim, Keith Nabors and Jacob White. IEE Transactions on Microwave Theory and Thechniques, 40(7):11, 1992.

8. Keith Nabors and Jacob White. IEE Transactions on Computer-Aided Design, 10(11):13, 1991.

9. Friedel Hartmann. Introduction to Boundary Elements. Springer-Verlag, first edition, 1989.

10. Mark F. Gyure and Paul D. Beale. Physical Review B, 46(7):11, 1992.

11. Paul D. Beale and P. M. Duxbury 1988 Physical Review B 37

12. Horst B and Kim S A Graph distance metric based on the maximal common subgraph 1998 Pattern Recognition Letters 19 255.

13. M.J. Newman, SIAM review, 45 167.

14. S. Caorsi, D. Moreno and F. Sidoti, Theoretical and Numerical Treatment of Surface Integrals Involving the Free-Space Green's Function. IEEE transactions on antennas and propagation 1993 41

15. Jarvenpaa, S., Taskinen, M. Numerical evaluation of integrals involving the free-space green's function multiplied with a polynomial shape function on a triangle in 3D Antennas and Propagation Society International Symposium 2002 IEEE

16. M. Pascoal and E. Martins. A new implementation of Yen's ranking loopless paths algorithm 2003 4OR – Quarterly Journal of the Belgian, French and Italian Operations Research Societies

17. Wang L and Dang Z-M 2005 Appl. Phys. Lett. 87 042903

18. Ahmad K and Pan W 2006 Appl. Phys. Lett. 89 13312

19. Pötschke P, Dudkin S M and Alig I 2003 Polymer 44 5023

20. Pötschke P, Bhattacharyya A R and Janke A 2004 Carbon 42 965

21. Munson-McGee S H 1991 Phys Rev B 43 331

22. Sheng-Hong Y, Zhi-Min D, Mei-Juan J, Hai-Ping X. Applied Physics Letters 2007;91:212901.

23. Al-Saleha MH, Sundarara U. A review of vapor grown carbon nanofiber/polymer conductive composites. Carbon 2009;47.2

24. Balberg I. Tunneling and nonuniversal conductivity in composite materials. Physical Review Letters 1987;59:1305.

25. Du F, Fischer JE, Winey KI. Effect of nanotube alignment on percolation conductivity in carbon nanotube/polymer composites. Physical Review B 2005;72:121404.

26. Ning H, Masuda Z, Cheng Y, Yamamoto G. Nanotechnology 2008;19:215701.

27. Fu M, Yu Y, Xie JJ, Wang LP, Fan MY, Jiang SL, Zeng YK. Significant influence of film thickness on the percolation threshold of multiwall carbon nanotube/low density polyethylene composite films. Applied Physics Letters 2009;94:012904.

28. Stauffer, D. and A. Aharony, Introduction to Percolation Theory. 1992, London: Taylor and Francis.

29. Bergrman and Stroud, Physical Review B, 1982. 25: p. 2061.

30. Kirkpatrick, S., Review of Modern Physics, 1973. 45: p. 574–88.

31. Herrmann, H.J. and B. Derrida, Phyisical Review B, 1984. 30(7): p. 4080.

32. Myroshnychenko, V. and C. Brosseau, Journal of Physics D: Applyed Physics, 2008(41): p. 095401.

33. Berhan, L. and A.M. Sastry, Modeling percolation in high-aspect-ratio fiber systems. I. Soft-core versus hard-core models. Physical Review E (Statistical, Nonlinear, and Soft Matter Physics), 2007. 75(4): p. 041120-8.

34. Berhan, L. and A.M. Sastry, Modeling percolation in high-aspect-ratio fiber systems. II. The effect of waviness on the percolation onset. Physical Review E (Statistical, Nonlinear, and Soft Matter Physics), 2007. 75(4): p. 041121-7.

35. Kesten, H., Notices of the American math society. 2005. 53(5).

36. Wu, J. and D.S. McLachlan, Scaling behavior of the complex conductivity of graphite-boron nitride percolation systems. Physical Review B, 1998. 58(22): p. 14880.

37. Z.-M. Dang LW, Y. Yin, Q. Zhang, Q.-Q. Lei,. Giant Dielectric Permittivities in Functionalized Carbon-Nanotube/ Electroactive-Polymer Nanocomposites. Advanced Materials 2007;19:852.